Cellular/Molecular

Specific Targeting of Pro-Death NMDA Receptor Signals with Differing Reliance on the NR2B PDZ Ligand

Francesc X. Soriano,[1,2]* Marc-Andre Martel,[1,2]* Sofia Papadia,[1,2] Anne Vaslin,[3] Paul Baxter,[1,2] Colin Rickman,[1] Joan Forder,[4] Michael Tymianski,[4] Rory Duncan,[1] Michelle Aarts,[5] Peter G. H. Clarke,[3] David J. A. Wyllie,[1,2] and Giles E. Hardingham[1,2]

Centres for [1]Integrative Physiology and [2]Neuroscience Research, University of Edinburgh, Edinburgh EH8 9XD, United Kingdom, [3]Département de Biologie Cellulaire et de Morphologie, Université de Lausanne, CH-1015 Lausanne, Switzerland, [4]Department of Neurosurgery, Toronto Western Hospital, Toronto, Ontario, Canada M5T 2S8, and [5]Centre for the Neurobiology of Stress, University of Toronto at Scarborough, Scarborough, Ontario, Canada M1C 1A4

NMDA receptors (NMDARs) mediate ischemic brain damage, for which interactions between the C termini of NR2 subunits and PDZ domain proteins within the NMDAR signaling complex (NSC) are emerging therapeutic targets. However, expression of NMDARs in a non-neuronal context, lacking many NSC components, can still induce cell death. Moreover, it is unclear whether targeting the NSC will impair NMDAR-dependent prosurvival and plasticity signaling. We show that the NMDAR can promote death signaling independently of the NR2 PDZ ligand, when expressed in non-neuronal cells lacking PSD-95 and neuronal nitric oxide synthase (nNOS), key PDZ proteins that mediate neuronal NMDAR excitotoxicity. However, in a non-neuronal context, the NMDAR promotes cell death solely via c-Jun N-terminal protein kinase (JNK), whereas NMDAR-dependent cortical neuronal death is promoted by both JNK and p38. NMDAR-dependent pro-death signaling via p38 relies on neuronal context, although death signaling by JNK, triggered by mitochondrial reactive oxygen species production, does not. NMDAR-dependent p38 activation in neurons is triggered by submembranous Ca^{2+}, and is disrupted by NOS inhibitors and also a peptide mimicking the NR2B PDZ ligand (TAT-NR2B9c). TAT-NR2B9c reduced excitotoxic neuronal death and p38-mediated ischemic damage, without impairing an NMDAR-dependent plasticity model or prosurvival signaling to CREB or Akt. TAT-NR2B9c did not inhibit JNK activation, and synergized with JNK inhibitors to ameliorate severe excitotoxic neuronal loss *in vitro* and ischemic cortical damage *in vivo*. Thus, NMDAR-activated signals comprise pro-death pathways with differing requirements for PDZ protein interactions. These signals are amenable to selective inhibition, while sparing synaptic plasticity and prosurvival signaling.

Key words: **NMDA receptor; neuronal death; PDZ domains; stroke; calcium; mitochondria; neuroprotection; nitric oxide; protein kinase; signal transduction**

Introduction

A high and prolonged rise in the extracellular glutamate concentration kills central neurons (Olney, 1969). During an ischemic episode, glutamate levels build up as a result of synaptic release and impaired and/or reversed uptake mechanisms (Camacho and Massieu, 2006), which induce Ca^{2+}-dependent cell death via excessive activation of NMDA glutamate receptors (NMDARs) (Arundine and Tymianski, 2004). Excessive NMDAR activity can lead to cell death in other acute episodes such as mechanical trauma, and may contribute to neurodegeneration in Alzheimer's disease (Chohan and Iqbal, 2006). The destructive effects of excessive NMDAR activity are in contrast to the prosurvival effects of physiological NMDAR activity (Ikonomidou and Turski, 2002; Hardingham and Bading, 2003; Papadia and Hardingham, 2007). Elimination of NMDAR activity *in vivo* causes widespread apoptosis and enhances trauma-induced injury in developing neurons (Gould et al., 1994; Ikonomidou et al., 1999; Adams et al., 2004). In the adult CNS, NMDAR blockade exacerbates neuronal loss when applied after traumatic brain injury and during ongoing neurodegeneration (Ikonomidou et al., 2000), and prevents the survival of newborn neurons in the adult dentate gyrus (Tashiro et al., 2006). Molecular mechanisms of synaptic NMDAR-dependent neuroprotection are beginning to be elucidated (Hetman and Kharebava, 2006; Papadia and Hardingham, 2007; Zhang et al., 2007; Papadia et al., 2008). Thus, responses of neurons to NMDAR activity follow a bell-shaped curve: both too much and too little are potentially harmful. The central role of the NMDAR in CNS physiology offers an explanation as to why clinical treatment of stroke with NMDAR antagonists has failed because of poor tolerance and efficacy (Ikonomidou and Turski, 2002; Muir, 2006). It would be desirable to block pro-death

Received Aug. 26, 2008; accepted Aug. 28, 2008.

This work was supported by the EC FP6 STRESSPROTECT (LHSM-CT-2004-005310), The Wellcome Trust, Biotechnology and Biological Sciences Research Council, and Grant 7057.2 BTS-LS from the Swiss Commission for Technology and Innovation and the Network of European Neuroscience Institutes. G.E.H. is supported by a Royal Society University Research Fellowship. We thank Christophe Bonny for D-JNKI1, Mike Murphy for MitoQ, Hidenori Ichijo and Anne Stephenson for plasmids, Rudolf Kraftsik for help with statistics, and Sonia Naegele for technical assistance.

*F.X.S. and M.-A.M. contributed equally to this work.

Correspondence should be addressed to Giles E. Hardingham at the above address. E-mail: giles.hardingham@ed.ac.uk.

DOI:10.1523/JNEUROSCI.1207-08.2008

 0270-6474/08/2810696-15$15.00/0

NMDAR signaling in stroke, without affecting prosurvival signaling or indeed synaptic plasticity, many forms of which are mediated by NMDAR activation.

In neurons, Ca^{2+} influx through NMDARs promotes cell death more efficiently than through other Ca^{2+} channels (Tymianski et al., 1993; Arundine and Tymianski, 2004), suggesting that proteins responsible for Ca^{2+}-dependent excitotoxicity reside within the NMDAR signaling complex (NSC). A role for the NSC in mediating NMDAR-dependent death was shown in the case of the PDZ proteins neuronal nitric oxide synthase (nNOS) and PSD-95 (Aarts et al., 2002). PSD-95 is linked to the C-terminal PDZ ligand of NR2, and also binds to nNOS. When the interaction of NR2B and PSD-95 is disrupted, the NMDAR becomes uncoupled from nNOS activation, reducing (but not eliminating) NMDAR-dependent excitotoxicity (Aarts et al., 2002). The important role of nNOS and PSD-95 above any other PDZ proteins in mediating NMDAR-dependent excitotoxicity was recently demonstrated (Cui et al., 2007).

The attractiveness of the NSC as a therapeutic target is questioned by two issues. First, it is not clear whether NSC components can be disrupted without affecting prosurvival or plasticity signaling. Second, NMDAR-dependent cell death can be reconstituted in non-neuronal cells lacking the NSC simply by expressing NMDARs (Cik et al., 1993; Anegawa et al., 2000), which shows that certain NMDAR-induced death pathways do not require the NSC.

We have investigated both these issues with the aim of developing an effective anti-excitotoxic strategy that spares prosurvival and plasticity signaling, focusing on two key mediators of excitotoxicity: the stress-activated protein kinases (SAPKs) p38 mitogen-activated protein kinase (MAPK) and c-Jun N-terminal protein kinase (JNK) (Kawasaki et al., 1997; Borsello et al., 2003; Rivera-Cervantes et al., 2004). We find that these death pathways have differing requirements for the NSC and can be disrupted to great effect *in vivo* and *in vitro* without impacting prosurvival signaling or a model of NMDAR-dependent synaptic plasticity.

Materials and Methods

Neuronal cultures, stimulations, and assessment of nuclear morphology. Cortical neurons from embryonic day 21 Sprague Dawley rats were cultured as described previously (Bading and Greenberg, 1991) except that growth medium was comprised of Neurobasal A medium with B27 (Invitrogen), 1% rat serum, and 1 mM glutamine. Experiments were performed after a culture period of 9–10 d, during which neurons developed a rich network of processes, expressed functional NMDA-type and AMPA/kainate-type glutamate receptors, and formed synaptic contacts (Hardingham et al., 2001a, 2002). Before stimulations, neurons were transferred from growth medium to a medium containing 10% MEM (Invitrogen), 90% salt-glucose-glycine (SGG) medium (Bading et al., 1993) (114 mM NaCl, 0.219% $NaHCO_3$, 5.292 mM KCl, 1 mM $MgCl_2$, 2 mM $CaCl_2$, 10 mM HEPES, 1 mM glycine, 30 mM glucose, 0.5 mM sodium pyruvate, and 0.1% phenol red; osmolarity, 325 mOsm/L). Neurons were treated with NMDA in the presence or absence of tetrodotoxin (TTX; 1 μM; EMD Biosciences). To trigger NMDAR-dependent excitotoxic cell death, neurons were exposed to NMDA or glutamate [in the presence of nifedipine (5 μM; Tocris Bioscience)] in our standard trophically deprived medium (90% SGG and 10% MEM) for 1 h, after which neurons were washed once and returned to fresh medium. Neurons that die in response to exposure to excitotoxic levels of glutamate exhibit swollen cell bodies and pyknotic nuclei with small irregular chromatin clumps, a characteristic of necrotic cell death as opposed to apoptotic-like death (Fujikawa et al., 2000) [for example pictures, see Hardingham et al. (2002)]. Cell death was determined 24 h later by counting the number of 4′,6′-diamidino-2-phenylindole (DAPI)-stained pyknotic/necrotic nuclei as a percentage of the total. For each treatment, 800–1000 cells were scored across several random fields within three to four independent experiments. When used, carbonyl cyanide *p*-trifluoromethoxyphenylhydrazone (FCCP) (1 μM) and oligomycin (10 mM) were added 5 min before stimulation. TAT-based peptides were used at 2 mM and were added 1 h before stimulation, as were all pharmacological inhibitors. 10-(6′-Ubiquinonyl) decyltriphenylphosphonium bromide (MitoQ) and its decyltriphenylphosphonium bromide (DTPP) targeting moiety control (gifts from Dr. Mike Murphy, University of Cambridge, Cambridge, UK) were used at 5 μM and added 1 h before stimulation.

Transfection and luciferase assays. AtT20 cells (European Collection of Cell Cultures number 87021902) were maintained in DMEM medium (Invitrogen) supplemented with 10% fetal bovine serum (Invitrogen) and antibiotics. AtT20 cells were transiently transfected in 24-well plates with pCis vectors containing full-length mouse cDNAs encoding for the NR1-1a (hereafter referred to as NR1) and NR2B subunits, along with a SV40-luciferase plasmid in a 2:2:1 ratio, respectively. Transfection was done using a total of 0.5 μg of cDNA per well and 2.33 μl/well of Lipofectamine reagent (2 μg/ml) or Lipofectamine 2000 (1 μg/ml; both from Invitrogen). Transfection was achieved following the manufacturer's instructions and using the OptiMEM I medium (Invitrogen). Transfection efficiency was ~5–10%. At the end of the transfection period, the mixture was replaced with fresh OptiMEM I containing 50 μM D-APV (Tocris Bioscience) to prevent spontaneous NMDAR-induced cell death. Assays were performed 16–24 h after the end of transfection. Transfected AtT20 cells were stimulated with various glutamate concentrations for 5–7 h, with drugs being preapplied for at least 1 h before agonist application. After the incubation period, the medium was removed, and 90 μl of Steady-Glo Luciferase Assay Kit (Promega) mixture was added to an equal amount of fresh medium. Cells were allowed to lyse at room temperature for 10 min and then transferred to opaque white 96-well plates (Greiner Bio-One). Luciferase activity was measured by assaying the chemiluminescence using FLUOstar Optima plate reader (BMG Labtech). The relative light units were converted to percentage of cell death compared with control (100%), and the minimum luminescence value was normalized to 0% to account for transfection efficiency variations.

To confirm the existence of functional NMDARs in the transfected AtT20 cells, recordings of agonist-evoked whole-cell currents in NMDAR-expressing AtT20 cells were made 18–72 h after transfection using a Mg^{2+}-free external solution. Agonists (100 μM glutamate and 100 μM glycine) were applied with an independent line positioned near the whole-cell clamped cell to achieve quick stimulation and to minimize exposure of adjacent cells to agonists. Data were filtered at 1 kHz and digitized at 5 kHz for subsequent off-line analysis.

Neurons were transfected at day *in vitro* 8 (DIV8) using Lipofectamine 2000 as described previously (McKenzie et al., 2005). Transfection efficiency was ~2–5%. More than 99% of enhanced green fluorescent protein (eGFP)-expressing transfected neurons were NeuN positive, and <1% were GFAP positive (Papadia et al., 2008), confirming their neuronal identity. For CRE-reporter assays, neurons were treated with bicuculline 24 h after transfection with 0.5 μg of CRE-Luc plus 0.1 μg of pTK-*Renilla*. Bicuculline-induced activity was terminated [by (+)-5-methyl-10,11-dihydro-5*H*-dibenzo[a,d]cyclohepten-5,10-imine maleate (MK-801) and TTX] after 30 min or 1 h, and luciferase expression was analyzed 6–7 h later. Luciferase assays were performed using the Dual-Glo assay kit (Promega) with firefly luciferase-based CRE-reporter gene activity normalized to the *Renilla* control in all cases.

^{45}Calcium assay: measurement of total, cytoplasmic, and vesicular Ca^{2+} loads. Nifedipine (5 μM) was added 1 h before the experiment to prevent calcium entry through voltage-gated calcium channels. Cortical neurons and NMDAR-expressing AtT20 cells were then stimulated for 10 min at 37°C with glutamate, using medium enriched with 30–50 MBq/L $^{45}Ca^{2+}$. After the 10 min incubation, cells were washed once with fresh medium supplemented with kynurenate (10 mM) and magnesium (10 mM). For measuring total Ca^{2+} load, cells were simply lysed with PBS containing 1% Triton and transferred to scintillation vials. To measure cytoplasmic and vesicular Ca^{2+} load separately, we followed an established procedure (Ward et al., 2005). Briefly, cytoplasmic Ca^{2+} was released from the cells by adding 100 μl of Ca^{2+}-free medium containing

0.01% digitonin for 2 min, then collected for counting. The remaining vesicular Ca^{2+} was then measured by adding PBS/Triton as before. After addition of 1 ml of scintillation liquid (VWR), Ca^{2+} entry in counts per minute was quantified using a Beckman LS6500 scintillation counter. Data from each experiment were normalized for the amount of $^{45}Ca^{2+}$ activity used, and the basal radioactivity count from the nonstimulated cells was subtracted from each subsequent condition.

Recordings and analysis of miniature EPSC and spontaneous EPSC frequency. For miniature EPSC (mEPSC) recordings, neurons were placed in medium containing control solution with or without 50 μM bicuculline (Tocris Bioscience) for 15 min and then returned to control medium for 30 min. Coverslips were then transferred into a recording chamber containing artificial CSF (aCSF) made of the following (in mM): 150 NaCl, 2.8 KCl, 10 HEPES, 2 $CaCl_2$, 1 $MgCl_2$, and 10 glucose, pH 7.3 (320–330 mOsm). Patch pipettes were made from thick-walled borosilicate glass (Harvard Apparatus) and filled with a K-gluconate-based internal solution containing the following (in mM): 155 K-gluconate, 2 $MgCl_2$, 10 Na-HEPES, 10 Na-Pi/creatine, 2 Mg_2-ATP, and 0.3 Na_3-GTP, pH 7.3 (300 mOsm). These electrodes were coated with Sylgard 184 resin (Dow Corning), and their tips were fire polished for a final resistance between 5 and 10 MΩ.

mEPSCs were recorded (Baxter and Wyllie, 2006) using an Axopatch-1C amplifier (Molecular Devices) at room temperature (21 ± 2°C) with the aCSF supplemented with 300 nM TTX and 50 μM picrotoxin (both from Tocris Bioscience). Events were recorded for 5–10 min (minimum of 300 events) from neurons clamped at −70 mV. Recordings were rejected if the cell holding current was higher than −100 pA or if series resistances drifted by >20% of their initial value and were <35 MΩ. For data analysis, the tape-recorded mEPSCs were filtered at 2 kHz and digitized at 10 kHz using WinEDR version 6.1 software (John Dempster, University of Strathclyde, Glasgow, UK). Files were then analyzed as described previously (Baxter and Wyllie, 2006) with MiniAnalysis software (Synaptosoft). mEPSCs were manually selected with a minimum amplitude threshold of 6 pA (approximately two times the baseline noise level) and a maximum peak rising-time threshold of 5 ms.

Recordings of spontaneous EPSCs (sEPSCs) were obtained using an aCSF with 3 mM $CaCl_2$ to obtain a reliably high level of spontaneous events in the cultures. Activity was recorded for 3 min while holding the neuron at −70 mV. Only sEPSCs >200 pA and spaced by >1 s were selected for frequency analysis.

Western blotting and antibodies. Total cell lysates were boiled at 100°C for 5 min in 1.5× sample buffer (1.5 M Tris, pH 6.8, 15% glycerol, 3% SDS, 7.5% β-mercaptoethanol, and 0.0375% bromophenol blue). Gel electrophoresis and Western blotting were performed using the Xcell Surelock system (Invitrogen) with precast gradient gels (4–20%) according to the manufacturer's instructions. The gels were blotted onto polyvinylidene difluoride membranes, which were blocked for 1 h at room temperature with 5% (w/v) nonfat dried milk in TBS with 0.1% Tween 20. The membranes were incubated at 4°C overnight with the primary antibodies diluted in blocking solution: anti-phospho-Jun Ser73 (1:500; Cell Signaling Technology), phospho-Jun Ser63 (1:500; Cell Signaling Technology), Jun (1:1000; BD Transduction Laboratories), phospho-p38 Thr180/Tyr182 (1:400; Cell Signaling Technology), p38 (1:1000; Santa Cruz Biotechnology) β-tubulin isotype III (1:125,000; Sigma), phospho-Akt Ser473 (1:500; Cell Signaling Technology), Akt (1:500; Cell Signaling Technology), p-ASK1 Thr845 (1:1000; Cell Signaling Technology), p-MKK4 Thr261 (1:1000; Cell Signaling Technology), hemagglutinin (HA) (1:1000; Cell Signaling Technology), p-p44/42 MAPK Thr202/Tyr204 (p-ERK1/2; 1:2000; Cell Signaling Technology), PSD-95 [1:1000; Abcam (goat)], and nNOS [1:500; Abcam (goat)]. For visualization of Western blots, HRP-based secondary antibodies were used followed by chemiluminescent detection on Kodak X-Omat film. Western blots were analyzed by digitally scanning the blots, followed by densitometric analysis (ImageJ). All analysis involved normalizing to a loading control, either to the unmodified version of the modification under study (e.g., phospho-p38 normalized to p38) or to β-tubulin isotype III.

RNA isolation, reverse transcription-PCR, and quantitative PCR. RNA was isolated using the Qiagen RNeasy isolation reagents (including the optional DNase treatment) after passage of the cells through a QiaShredder column. For quantitative PCR (qPCR), cDNA was synthesized from 1–3 μg of RNA using the Stratascript QPCR cDNA Synthesis kit (Stratagene) according to the manufacturer's instructions. Briefly, the required amount of RNA (up to 3 μg) was diluted in RNase-free water (up to 7 μl final volume) and mixed on ice with 1× cDNA Synthesis master mix (10 μl), random primers:oligo-dT primers (3:1) [total, 2 μl (200 ng)], and either 1 μl of reverse transcriptase/RNase block enzyme mixture [for reverse transcription (RT) reactions] or 1 μl of water (for no-RT control reactions). Reaction mixtures were mixed and spun down and incubated for 2 min at 25°C, 40 min at 42°C, and 5 min at 95°C. cDNA was stored at −20°C. Dilutions of this cDNA were used subsequently for real-time PCR [cDNA equivalent to 6 ng of initial RNA per 15 μl qPCR for all genes except glyceraldehyde-3-phosphate dehydrogenase (GAPDH); cDNA equivalent to 2 ng of initial RNA per 15 μl reaction for GAPDH]. qPCR was performed in an Mx3000P QPCR System (Stratagene) using Brilliant SYBR Green QPCR Master Mix (Stratagene) according to the manufacturer's instructions. Briefly, the required amount of template was mixed on ice with 1× Brilliant SYBR Green Master Mix, the required concentration of forward and reverse primers, 30 nM ROX passive reference dye, and water to the required reaction volume. Technical replicates as well as no-template and no-RT negative controls were included, and at least three biological replicates were studied in each case. The sequence and concentration of the primers used are as follows: rat Adcyap1, forward (F), 5′-ATGTGTAGCGGAGCAAGG-3′ (200 nM); reverse (R), 5′-GAGTGGCGTTTGGTAAGG-3′ (200 nM); rat GAPDH, F, 5′-AGAAGGCTGGGGCTCACC-3′ (200 nM); R, 5′-AGTTGGTGGTGCAGGATGC-3′ (100 nM). The cycling program was 10 min at 95°C; 40 cycles of 30 s at 95°C, 40 s at 60°C with detection of fluorescence, and 30 s at 72°C; and 1 cycle (for dissociation curve) of 1 min at 95°C and 30 s at 55°C with a ramp up to 30 s at 95°C (ramp rate, 0.2°C/s) with continuous detection of fluorescence on the 55–95°C ramp. The data were analyzed using the MxPro QPCR analysis software (Stratagene). Expression of the gene of interest was normalized to GAPDH, a commonly used control.

Immunoprecipitation. For each treatment, 3 × 35 mm dishes (~1.5×10^6 neurons) transfected with pHA-ASK1 or control (globin) expression vector were lysed in 400 ml of lysis buffer [0.05 M Tris base, 0.9% NaCl, pH 7.6, and 0.5% Triton X-100 plus Protease Inhibitors Cocktail Set III (1:100; EMD Biosciences) and phosphatase inhibitor cocktails 1 and 2 (1:500; Sigma)]. Lysate was clarified at 16,000 × *g* for 15 min at 4°C. The supernatant was then precleared with 25 ml of 50% Protein A Sepharose (Sigma) for 1 h at 4°C, and after a brief spin, the pellet was discarded. Ten percent of the supernatant was retained as input for normalization purposes. The remainder was incubated overnight with 1:100 dilution of anti-HA antibody (Cell Signaling Technology) at 4°C. The immunocomplex was precipitated with 25 ml of 50% Protein A Sepharose for 1 h at 4°C. The pellet was washed three times in lysis buffer, then boiled for 10 min in 25 ml of 1.5× sample loading buffer (1.5 M Tris, pH 6.8, 15% glycerol, 3% SDS, 7.5% β-mercaptoethanol, and 0.0375% bromophenol blue) before gel electrophoresis and Western blotting.

Neonatal focal ischemia models. All animal procedures were in compliance with the directives of the Swiss Academy of Medical Science and were authorized by the veterinary office of the Canton of Vaud. D-JNKI1 and Tat-NR2B9c peptides were dissolved in saline and administered intraperitoneally. Because the therapeutic time window with D-JNKI1 has been shown to be 12 h, with maximal protection at 6 h for middle cerebral artery occlusion (MCAO) in postnatal day 14 (P14) rats, we administered D-JNKI1 at 6 h after the onset of ischemia; the chosen dose was 0.3 mg/kg (i.p.) because pilot experiments showed this to be optimal (A. Vaslin, unpublished work). In contrast, Tat-NR2B9c (7.5 mg/kg) was given 30 min before cerebral ischemia, because the therapeutic window was unknown. Control animals received saline. Focal ischemia was induced in 12-d-old male Sprague Dawley rats. Anesthesia was induced with 2.5% isoflurane in a chamber and maintained during the operation with a mask using 2.5% isoflurane. MCAO was performed as described previously (Borsello et al., 2003). A more severe model (MCAO+) was performed (Renolleau et al., 1998). Briefly, the main (cortical) branch of the left middle cerebral artery was electrocoagulated just below the bifurcation of the MCA into frontal and parietal branches (as per the MCAO model). The left common carotid artery was then occluded by means of

a clip for 90 min, during which time the rat pups were maintained at 37°C in the induction chamber (2.5% isoflurane). The arterial clip was then removed, and the restoration of carotid blood flow was verified under a dissecting microscope before the skin incision was closed. Rat pups were transferred back to their mothers for a 24 h survival period. This severe model was compared with a milder model of permanent MCAO alone. With both models, the survival rate until the rats were killed was 100%.

The volume of the infarct was measured after 24 h of recirculation. Pups were heavily anesthetized with sodium pentobarbital and perfused through the ascending aorta with 4% paraformaldehyde in PBS, pH 7.4. Brains were removed, placed in PBS with 30% sucrose for ~15 h at 4°C, and then frozen in isopentane (−40°C). Cryostat coronal sections of 50 μm were stained with cresyl violet. The outline of the infarct was traced in each 10th slice using a computer-microscope system equipped with the Neurolucida program (MicroBrightField), and the infarct volume was calculated with NeuroExplorer (MicroBrightField). Lesions of <5 mm^3 (i.e., <10% of the mean lesion volume in saline controls) were considered artifactual (caused by technical error or vascular abnormality) and were eliminated from the main analysis. Three saline control rats were eliminated; however, reanalysis of the data confirmed that their inclusion would have changed none of the conclusions.

Three pial vessel occlusion model of ischemia. Male Sprague Dawley rats ($n = 8$ in each group) weighing between 280 and 320 g were used for this study. Except for 12 h immediately preceding surgery, all animals had *ad libitum* access to standard laboratory food before and after surgery. Experimental procedures were followed using guidelines established by the Canadian Council for Animal Care and have been approved by the University Health Network Animal Care Committee. Rats were anesthetized with a 0.5 ml/kg intramuscular injection of ketamine (100 mg/kg), acepromazine (2 mg/kg), and xylazine (5 mg/kg), supplemented with one-third of the initial dose as required. An anal temperature probe was inserted, and the animal was placed on a heating pad maintained at 37°C. The right external carotid artery (ECA) was cannulated with PE 10 polyethylene tubing for dye injections. The skull was exposed via a midline incision and scraped free of tissue, and the temporalis muscle was disconnected from the skull on the right side. Using a dissecting microscope and a pneumatic dental drill, a 6 × 4 mm cranial window was made over the right somatosensory cortex (2 mm caudal and 5 mm lateral to bregma) by drilling a rectangle through the skull and lifting off the piece of skull while keeping the dura intact. The tail vein was cannulated, and drugs were injected in the following order: Tat-NR2B9c peptide (7.5 mg/kg) or saline, 15 min before ischemia; p38 inhibitor 4-(4-fluorophenyl)-2-(4-hydroxyphenyl)-5-(4-pyridyl)1*H*-imidazole (SB202190) (30 mg/kg) or saline 10 min before ischemia. After being bathed with aCSF (maintained at 37°C), small boluses (10–20 μl) of the vital dye patent blue violet (10 mmol/L; Sigma) in normal saline were injected into the right external carotid artery to demonstrate transit through surface vessels of the cortex. Three critical arteriolar branches of the MCA around the barrel cortex were selected and electrically cauterized through the dura. After the cauterizations, the bolus injections and dye transits were repeated to ensure that transits through the cauterized arterioles were blocked. The rectangle of skull was replaced over the window, and the scalp was sutured. The catheter was removed from the ECA, the ECA was ligated, and the anterior neck was sutured. Each rat was returned to its individual cage under a heating lamp to maintain body temperature until the rat fully recovered. Food and water was supplied *ad libitum*. Twenty-four hours after surgery, animals were reanesthetized with 1 ml of pentobarbital, and the brain was quickly harvested. Coronal slices (2 mm) was taken through the brain and incubated in 2% triphenyltetrazolium chloride for 15 min at 37°C. Images were scanned, and brain slices were stored at −80°C.

Results

The NR2 PDZ ligand is not needed for NMDAR-mediated death in NMDAR-expressing AtT20 cells

We investigated cell death induced by NMDARs in the absence of the neuron-specific NMDAR signaling complex by expressing NR1/NR2B NMDARs in AtT20 cells (NR-AtT20 cells). The ultimate aim of these experiments is to determine how the NMDAR can signal to cell death in the absence of the neuronal NSC. Such signals are likely to be activated in neurons, in addition to signals that do require the NSC. Knowledge of both types of death signals may help in developing an effective anti-excitotoxic strategy. NR2B-containing NMDARs were chosen because the neurons used in this study for comparison are DIV9 cortical neurons whose NMDAR currents are NR2B dominated: whole-cell NMDAR currents are inhibited by 68 ± 6% by the NR2B-specific antagonist ifenprodil ($n = 6$; data not shown). Pure NR1/NR2B NMDARs are inhibited by ~80% by ifenprodil (Tovar and Westbrook, 1999), indicating that the majority of NMDARs in DIV9 cortical neurons are NR2B containing. Consistent with this, ifenprodil prevents NMDAR-dependent neuronal cell death (see below).

NR-AtT20 cells were subjected to patch-clamp analysis to confirm the formation of functional NMDARs (Fig. 1*A*). For viability studies, NR-AtT20 cells were cotransfected with a constitutively active luciferase vector (pSV40-Luc), which acts as a bioassay of NMDAR-dependent death in reconstituted systems (Boeckman and Aizenman, 1996) in which transfection efficiency is low (<10% in AtT20 cells). Because of a more positive resting membrane potential than neurons, spontaneous NMDAR activity can be high in NMDAR-expressing non-neuronal cells, so AtT20 cells were cultured after transfection in 50 μM APV. Glutamate treatment caused death of NR-AtT20 cells in a dose-dependent manner by outcompeting the APV (Fig. 1*B*), and was associated with Ca^{2+} influx (measured using a $^{45}Ca^{2+}$ tracer) (Fig. 1*C*). Death/loss of luciferase signal was blocked by MK-801 (Fig. 1*B*), and expression of NR2B alone (i.e., no NR1) failed to confer glutamate-induced death on AtT20 cells (Fig. 1*B*), confirming the need for functional NMDARs. To confirm that loss of luciferase signal corresponded to death, we corroborated these findings by studying the glutamate-dependent loss of eGFP-expressing NR-AtT20 cells (data not shown). To further test the validity of the technique, we first confirmed that in neurons, ifenprodil protected against glutamate-induced nuclear pyknosis (Fig. 1*D*) as well as preventing glutamate-induced loss of luciferase signal from neurons transfected with pSV40-Luc (Fig. 1*D*).

We next studied the expression of PSD-95 and nNOS in AtT20 cells, because these PDZ proteins are important in coupling the NMDAR to cell death in neurons, via the NR2 PDZ ligand (Cui et al., 2007). Western blot analysis revealed that levels of PSD-95 and nNOS were extremely low in AtT20 cells, compared with levels in equivalent amounts of neuronal protein extract (Fig. 1*E*). This suggests that the PDZ ligand of NR2B may not be important for NMDAR-dependent cell death in NR-AtT20 cells. To test this, AtT20 cells were transfected with vectors encoding NR1 plus a truncated form of NR2B lacking the PDZ ligand, NR2Btrunc (Rutter and Stephenson, 2000). Expression of NMDARs containing NR1 and NR2Btrunc triggered the same Ca^{2+} load (Fig. 1*F*) and also was as effective at promoting cell death (Fig. 1*G*) as expression of wild-type (WT) NMDARs. Thus, in the non-neuronal environment of an AtT20 cell, NMDARs can couple to cell death in the absence of PSD-95, nNOS, and the NR2B PDZ ligand, all components that contribute to NMDAR excitotoxicity in neurons (Cui et al., 2007).

Differing p38 MAPK dependency of NMDAR signaling to death in neurons versus NR-AtT20 cells

To investigate this apparent paradox, we studied the signals responsible for mediating NMDAR-dependent cell death in neu-

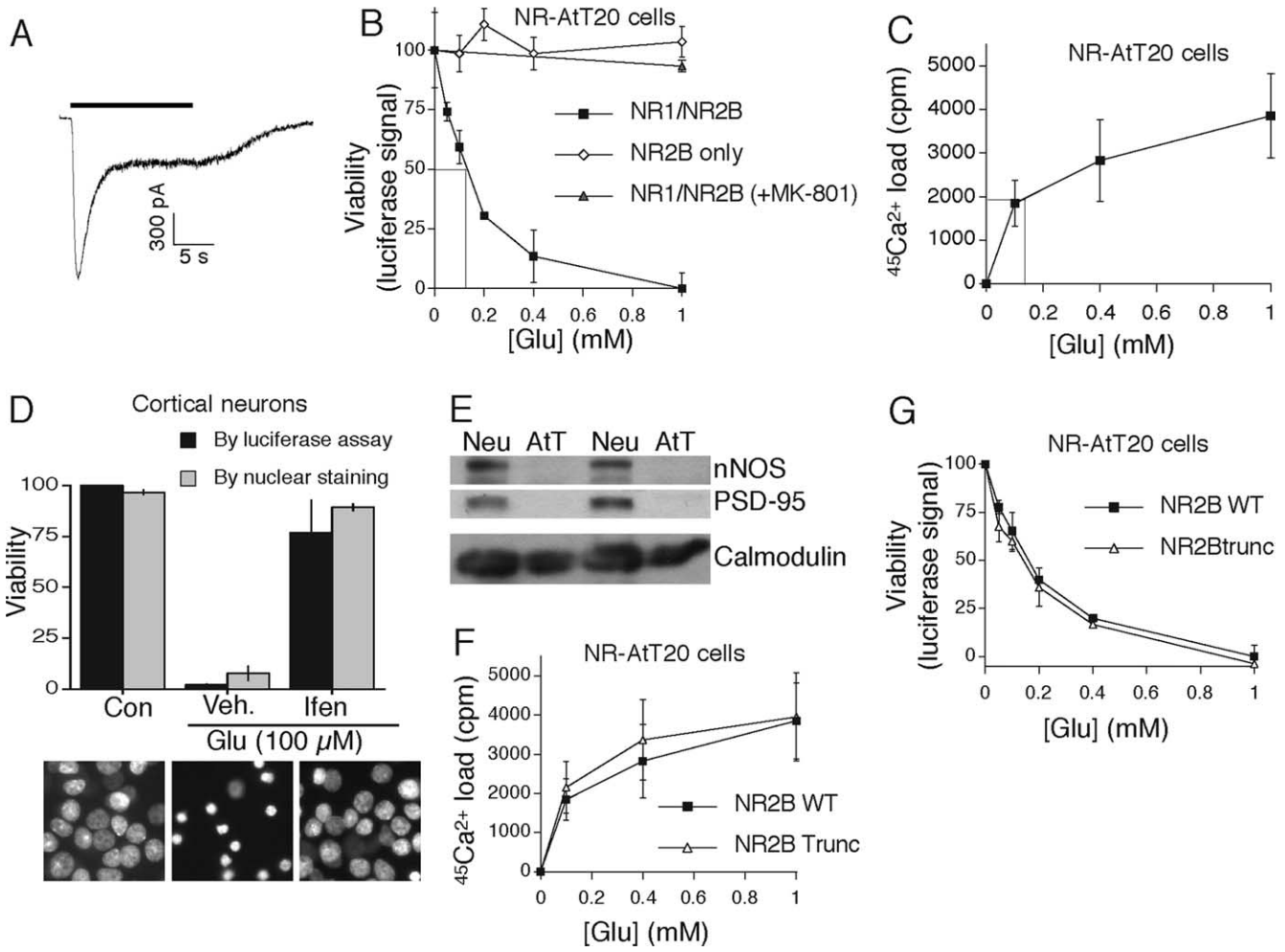

Figure 1. NMDAR-mediated Ca^{2+} influx can kill NMDAR-expressing AtT20 cells in the absence of PSD-95, nNOS, or the NR2 PDZ ligand. ***A***, AtT20 cells transfected with pNR1 and pNR2B plasmids express functional NMDARs. An example trace of agonist (100 μM glutamate; horizontal bar)-induced current in NMDAR-expressing AtT20 cells (NR-AtT20) is shown. ***B***, Reconstituting NMDAR-dependent cell death in AtT20 cells. NR-AtT20 cells were treated with glutamate (Glu) for 5–7 h. Cells were cotransfected with pSV40-Luc to enable viability to be measured by performing a luciferase assay on lysates. Mean ± SEM are shown in this and all subsequent figures ($n = 7$). ***C***, Measuring Ca^{2+} influx in NR-AtT20 cells. NR-AtT20 cells were incubated in $^{45}Ca^{2+}$-containing medium and treated with glutamate for 10 min ($n = 3$). ***D***, NR2B-containing NMDARs mediate excitotoxicity in DIV9 cortical neurons. Neurons were treated as indicated with glutamate with or without ifenprodil (Ifen; 3 μM). Neurons were transfected with pSV40-Luc to enable viability to be measured by a luciferase assay. In parallel, cell death was measured by counting pyknotic and nonpyknotic nuclei ($n = 3$). Bottom, Example pictures. Con, Control; Veh., vehicle. ***E***, Western analysis of nNOS and PSD-95 expression in equal quantities of protein extracts (by BCA assay) from AtT20 cells and cortical neurons. Calmodulin expression is also shown for comparison. ***F***, NMDARs containing a truncated NR2B (lacking the C-terminal 4 aa) mediate the same glutamate-dependent Ca^{2+} load as wild-type NR2B-containing NMDARs. AtT20 cells were transfected with pNR1 and either WT NR2B or NR2Btrunc. Twenty-four hours later, cells were incubated in $^{45}Ca^{2+}$-containing medium and treated with glutamate for 10 min ($n = 3$). ***G***, NMDARs containing NR2Btrunc are as effective at promoting glutamate-dependent cell death as wild-type NR2B-containing NMDARs. AtT20 cells were transfected with pNR1 and either WT NR2B or NR2Btrunc, plus pSV40-Luc. Twenty-four hours after transfection, cells were treated with glutamate for 5–7 h before luciferase assay ($n = 3$).

rons and NR-AtT20 cells, focusing on two key mediators of excitotoxicity, the SAPKs p38 and JNK (Kawasaki et al., 1997; Borsello et al., 2003). Under basal conditions, CNS neurons contain a pool of active JNK1, which does not influence viability, but can make it difficult to detect additional elevation of stress-activated JNK signaling with phospho-JNK antibodies (Coffey et al., 2002). Because this pool of JNK1 does not influence c-Jun phosphorylation, the latter was used as a sensitive metric of NMDAR-dependent JNK signaling (Fig. 2*A*). NMDAR-dependent c-Jun phosphorylation was inhibited by the JNK inhibitor 1,9-pyrazoloanthrone (SP600125), as well as the peptide inhibitor of JNK, D-JNKI1 (Borsello et al., 2003) (Fig. 2*A*), but not the p38 inhibitor 4-(4-fluorophenyl)-2-(4-methylsulfonylphenyl)-5-(4-pyridyl)-1*H*-imidazole (SB203580) (data not shown). SP600125 did not interfere with p38 autophosphorylation, in contrast to SB203580 (data not shown). In neurons, NMDAR activation induced both p38 and JNK signaling (Fig. 2*B*,*C*). Because we did not have access to neurons from JNK and p38 isoform-deficient mice, we tested the JNK/p38 inhibitors on NMDA-induced excitotoxicity to see whether these stress-activated protein kinases play a role in excitotoxicity in our system. Inhibitors of JNK and p38 reduced NMDAR-dependent cell death (Fig. 2*D*), indicating a contribution from both pathways.

In contrast to the effects of both JNK and p38 inhibitors on NMDAR-dependent neuronal death, JNK inhibition completely blocked NMDAR-dependent death of NR-AtT20 cells, whereas p38 inhibition had no effect (Fig. 2*E*). This is not because of absence of the p38 pathway in AtT20 cells: known SAPK activators, H_2O_2 and anisomycin, induced p38 activation (data not shown). The absence of a p38-dependent component of NMDAR-dependent death of NR-AtT20 cells indicated that neuron-specific signaling molecules may be required for p38 activation by NR2B-containing NMDARs.

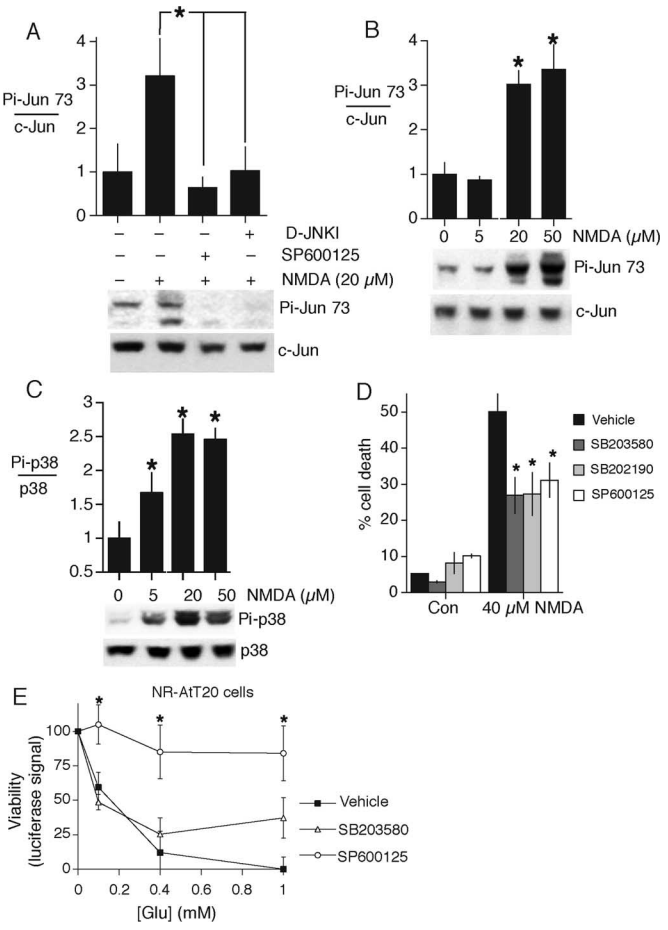

Figure 2. Differing p38 MAPK dependency of NMDAR pro-death signaling in neurons versus NR-AtT20 cells. ***A***, NMDAR-dependent c-Jun phosphorylation is JNK dependent. Cortical neurons were treated with the JNK inhibitors SP600125 (3 μM) and D-JNKI (2 μM) for 1 h before stimulation with NMDA (20 μM) for 30 min ($n = 3$). *$p < 0.05$, two-tailed Student's *t* test in this and all subsequent figures unless otherwise indicated. Western analysis of phospho-Jun (Ser73) levels was normalized to c-Jun levels ($n = 3$). ***B***, Western analysis of the dose–response of JNK-dependent Jun phosphorylation with NMDA stimulation in cortical neurons ($n = 5$). ***C***, Western analysis of the dose–response of p38 phosphorylation with NMDA stimulation in cortical neurons ($n = 5$). ***D***, NMDAR-mediated neuronal cell death is mediated by both JNK and p38 signaling. Neurons were treated with inhibitors of p38 (SB203580, 5 μM; SB202190, 5 μM) or JNK (SP600125, 1 μM) for 1 h before a 1 h excitotoxic insult. Neuronal loss was assessed after 24 h ($n = 3$). Con, Control. ***E***, NMDAR-dependent death of NR-AtT20 cells is totally JNK dependent. NR-AtT20 cells were treated with inhibitors of p38 (SB203580) or JNK (SP600125) for 1 h before glutamate treatment at the indicated concentrations. Luciferase assay was performed 5–7 h later. *$p < 0.05$, significant protection compared with control ($n = 3$).

NMDAR signaling to p38 MAPK involves NOS and requires only submembranous Ca^{2+} in neurons

In cortical neurons, p38 is an important downstream effector of NO toxicity (Ghatan et al., 2000), and in cerebellar granule cells NMDAR-dependent p38 activation is NOS-dependent (Cao et al., 2005). To determine whether NMDAR signaling to p38 is NOS-dependent in cortical neurons, we treated them with the NOS inhibitors L-*N*-nitroarginine methyl ester (L-NAME) and 7-nitroindazole (in arginine-free medium). Both inhibitors impaired p38 activation by NMDA (Fig. 3*A*) but not by H_2O_2 treatment (data not shown), indicating that NOS activation by NMDA is upstream of p38 in cortical neurons. To determine whether NO was sufficient to induce p38 activation in cortical neurons, we exposed them to the NO donor *S*-nitroso-*N*-acetylpenicillamine (SNAP), and found efficient p38 activation (Fig. 3*B*) that was transient, as is NMDAR-induced p38 activation (data not shown). The transient nature of p38 activation [phosphorylation followed by dephosphorylation (data not shown)] has been observed previously (Waxman and Lynch, 2005). The ability of NMDARs (specifically NR2B-containing NMDARs) to trigger p38 dephosphorylation (Krapivinsky et al., 2004; Waxman and Lynch, 2005) raises the question of whether NOS inhibitors act by blocking NMDAR-dependent p38 activation, or by slowing the p38 desphosphorylation. The former is more likely: even at 1 min stimulation, which is before full induction of p38, L-NAME inhibits NMDAR-dependent p38 activation (data not shown).

Whereas some NMDAR-dependent events, such as calcineurin-dependent NFAT (nuclear factor of activated T-cells) translocation, require bulk cytoplasmic Ca^{2+} increases, others, such as the Ras-ERK1/2 pathway, require only submembranous Ca^{2+} increases in the immediate vicinity of the NMDAR (Hardingham et al., 2001b). A sole requirement for submembranous Ca^{2+} would indicate receptor-proximal effectors of the NOS-p38 MAPK cascade. To determine this, we used a technique we previously established involving the cell-permeable Ca^{2+} chelator EGTA-AM and bicuculline (Hardingham et al., 2001b). Brief, easily bufferable, NMDAR-dependent Ca^{2+} transients were generated by network disinhibition using $GABA_A$ receptor blockade (bicuculline). These transients activated p38 in a MK-801-sensitive manner, just like NMDA bath application (Fig. 3*C*). We previously showed that preloading EGTA-AM at increasing concentrations before bicuculline stimulation blunts global Ca^{2+} transients at low doses of EGTA-AM, and abolishes them at 100 μM EGTA-AM (Hardingham et al., 2001b). The bicuculline stimulation is needed rather than bath NMDA, because the latter saturates the EGTA buffer. Because EGTA has a slow on-rate for Ca^{2+} binding, it allows increases in Ca^{2+} very near the site of entry, so bicuculline-induced bursting, reliant on evoked neurotransmitter release (a classical membrane-proximal Ca^{2+}-dependent process), still takes place (Hardingham et al., 2001b). Thus, EGTA-AM restricts intracellular Ca^{2+} transients to the immediate vicinity of the site of entry (the NMDAR). Strikingly, EGTA-AM loading did not compromise the activation of p38 after bicuculline treatment, even at 100 μM (Fig. 3*D*,*E*). In contrast, activation of Akt, another known NMDAR-activated signaling molecule, is abolished (Fig. 3*D*,*F*). We confirmed that p38 activation by bicuculline stimulation is NMDAR dependent (Fig. 3*C*), and NMDAR-dependent activation of p38 requires Ca^{2+} influx (no activation was observed in Ca^{2+}-free medium; data not shown). We conclude from Figure 3 that Ca^{2+} elevation in the immediate vicinity of the NMDAR is sufficient to trigger NOS-dependent p38 signaling in cortical neurons.

NMDAR signaling to p38 MAPK in neurons is disrupted by a peptide mimetic of the NR2B PDZ ligand

A recent study in cerebellar granule neurons showed that uncoupling of the NMDAR-associated scaffold protein PSD-95 from associated proteins, including nNOS (by overexpressing their interaction domains), impaired signaling to p38 (Cao et al., 2005). PSD-95 associates with the NMDAR via the C-terminal PDZ ligand of NR2. To determine whether the NR2 PDZ ligand plays a role in the NOS-dependent activation of p38 signaling in cortical neurons, we treated neurons with TAT-NR2B9c, a cell permeable (TAT-fused) peptide mimetic of the 9 C-terminal amino acids of NR2B, containing the PDZ ligand. TAT-NR2B9c disrupts NR2B/PSD-95 interactions, and uncouples the NMDAR from NO production (Aarts et al., 2002). TAT-NR2B9c strongly

impaired NMDAR-dependent p38 activation (Fig. 4*A*), without impairing NMDAR-dependent Ca^{2+} influx as assayed by $^{45}Ca^{2+}$ accumulation (supplemental Fig. S1, available at www.jneurosci.org as supplemental material). TAT-NR2B9c did not effect basal levels of p38 activity, nor did it effect p38 activation by a different stimulus (H_2O_2 treatment; data not shown). Thus, the effect of TAT-NR2B9c on p38 signaling appears to be specific to NMDAR-dependent p38 activation.

TAT-NR2B9c did not inhibit NMDAR-dependent activation of JNK signaling (Fig. 4*B*). Note that the effect of TAT-NR2B9c on p38 activation was observed at both the point of peak p38 activity (5 min) (Fig. 4*A*) and 30 min (data not shown), the time point at which the lack of JNK inhibition was observed.

Given that NMDAR-dependent death of NR-AtT20 cells is JNK dependent (Fig. 2*E*) and does not rely on the NR2 PDZ ligand (Fig. 1*G*), we would expect that TAT-NR2B9c would not impair NMDAR-dependent cell death of NR-AtT20 cells. This is indeed the case: TAT-NR2B9c had no effect on NMDAR-dependent death of NR-AtT20 cells (data not shown). Thus, the effect of TAT-NR2B9c on NMDAR signaling to cell death is specific to the p38 pathway, and further supports the idea that JNK signaling is independent of the NR2 PDZ ligand. Moreover, TAT-NR2B9c also impaired activation of ASK1 (Fig. 4*C*), a known upstream activator of p38 in neurons (Takeda et al., 2004) (as measured by analyzing Thr-854 phosphorylation). Together, the data in Figures 3 and 4*A–C* support the hypothesis that NMDAR-dependent activation of p38 can be triggered by submembranous Ca^{2+}, and requires the NR2 PDZ ligand to couple to associated proteins in cortical neurons.

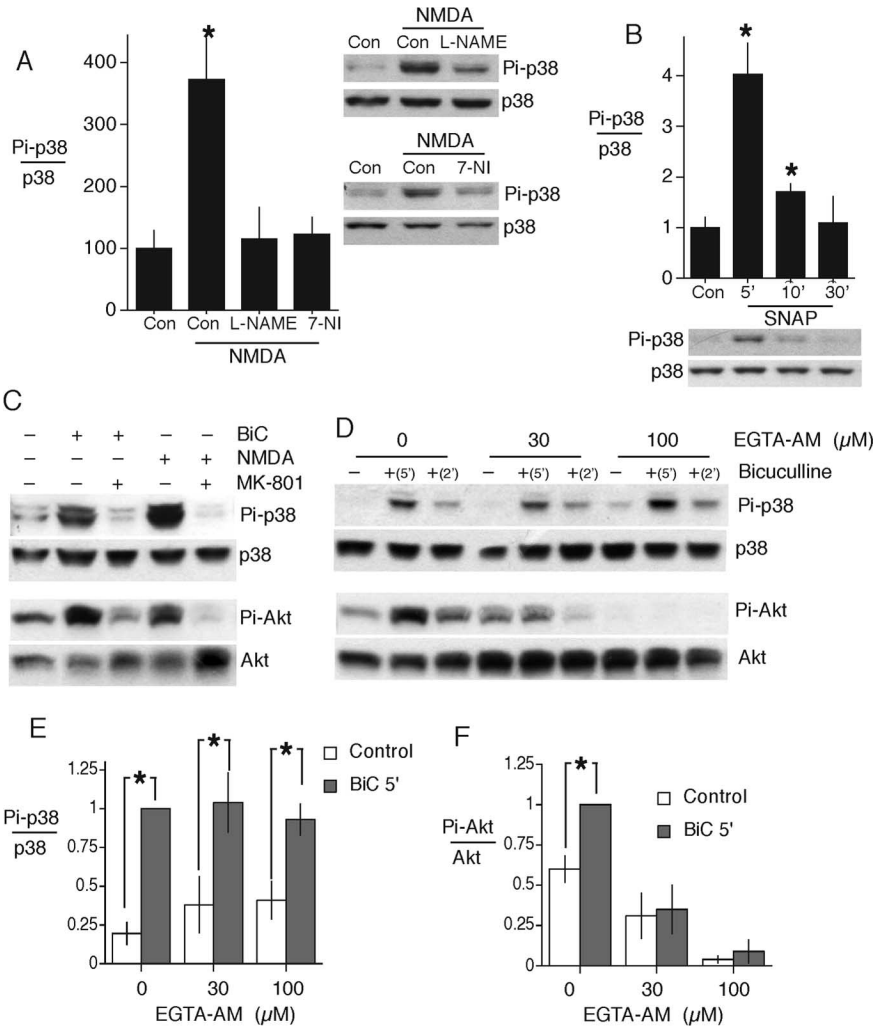

Figure 3. NMDAR signaling to p38 MAPK in cortical neurons involves NOS and requires only submembranous Ca^{2+}. ***A***, NMDAR-dependent p38 activation in cortical neurons is NOS dependent. Neurons were placed in arginine-free medium and treated with either vehicle or a NOS inhibitor for 1 h [L-NAME at 500 μM and 7-nitroindazole (7-NI) at 5 μM]. Neurons were then stimulated with NMDA (20 μM) for 5 min before harvesting and Western analysis ($n = 4$). Con, Control. ***B***, Nitric oxide donor SNAP is sufficient to induce p38 activation in cortical neurons. Neurons were treated with the NO donor SNAP (500 μM) for the indicated times before harvesting and Western analysis ($p < 0.05$ compared with untreated neurons; $n = 3–4$). ***C***, Bicuculline-induced synaptic activity promotes NMDAR-dependent p38 and Akt activation. Western analysis of p38 and Akt activation in cortical neurons was performed using phosphospecific antibodies. Neurons were stimulated with NMDA (20 μM) or bicuculline (BiC; 50 μM) for 5 min with or without MK-801 (10 μM). ***D–F***, Eliminating global Ca^{2+} transient by loading neurons with EGTA-AM does not affect p38 activation, but abolishes Akt activation. ***D***, Western analysis of p38 and Akt activation in neurons stimulated with bicuculline for 2 or 5 min. Before bicuculline stimulation, neurons were preloaded with EGTA-AM at room temperature for 20 min (Hardingham et al., 2001b). ***E***, Analysis of the effect of EGTA-AM on bicuculline-induced p38 activation ($n = 3$). ***F***, Analysis of the effect of EGTA-AM on bicuculline-induced Akt activation ($n = 3$).

Consistent with previous studies, TAT-NR2B9c reduced NMDAR-dependent neuronal death as assayed by studying nuclear pyknosis (Fig. 4*D*; example phase-contract pictures also shown). Using an alternative assay of cell viability, ATP levels, TAT-NR2B9c also reduced NMDAR-dependent neuronal death (Fig. 4*E*). We next investigated whether the neurons "protected" by TAT-NR2B9c were functional, focusing on the TAT-NR2B9c-treated neurons that were exposed to an ordinarily toxic dose of NMDA (40 μM). In current-clamp recordings, we injected current into the surviving cells (with 300 ms pulses at 1 Hz) to bring them to threshold. In current-clamp configuration, all surviving cells studied fired action potential bursts when depolarized beyond −40 mV, as was observed with non-NMDA-treated neurons (Fig. 4*F*). In voltage clamp, we also measured sEPSC frequency in surviving cells, to determine whether surviving neurons remained synaptically connected to other neurons. The prolonged nature of these sEPSCs presumably reflects the fact that these events are associated with action-potential bursts of activity that occur in the rest of the network of cultured neurons. In neurons treated with 40 μM NMDA alone, there was a severe decrease in sEPSC frequency of surviving cells (Fig. 4*G*), consistent with the large amount of cell death (each surviving neuron would be connected to fewer neurons). In contrast, neurons that are protected by TAT-NR2B9c after an excitotoxic insult exhibit no such reduction in sEPSC frequency (Fig. 4*G*), indicating that not only does TAT-NR2B9c prevent cell death, but that by this assay, overall connectivity and excitability of the neurons are preserved.

TAT-NR2B9c reduces focal ischemic brain damage in rats (Aarts et al., 2002), and the results above suggest that this may be

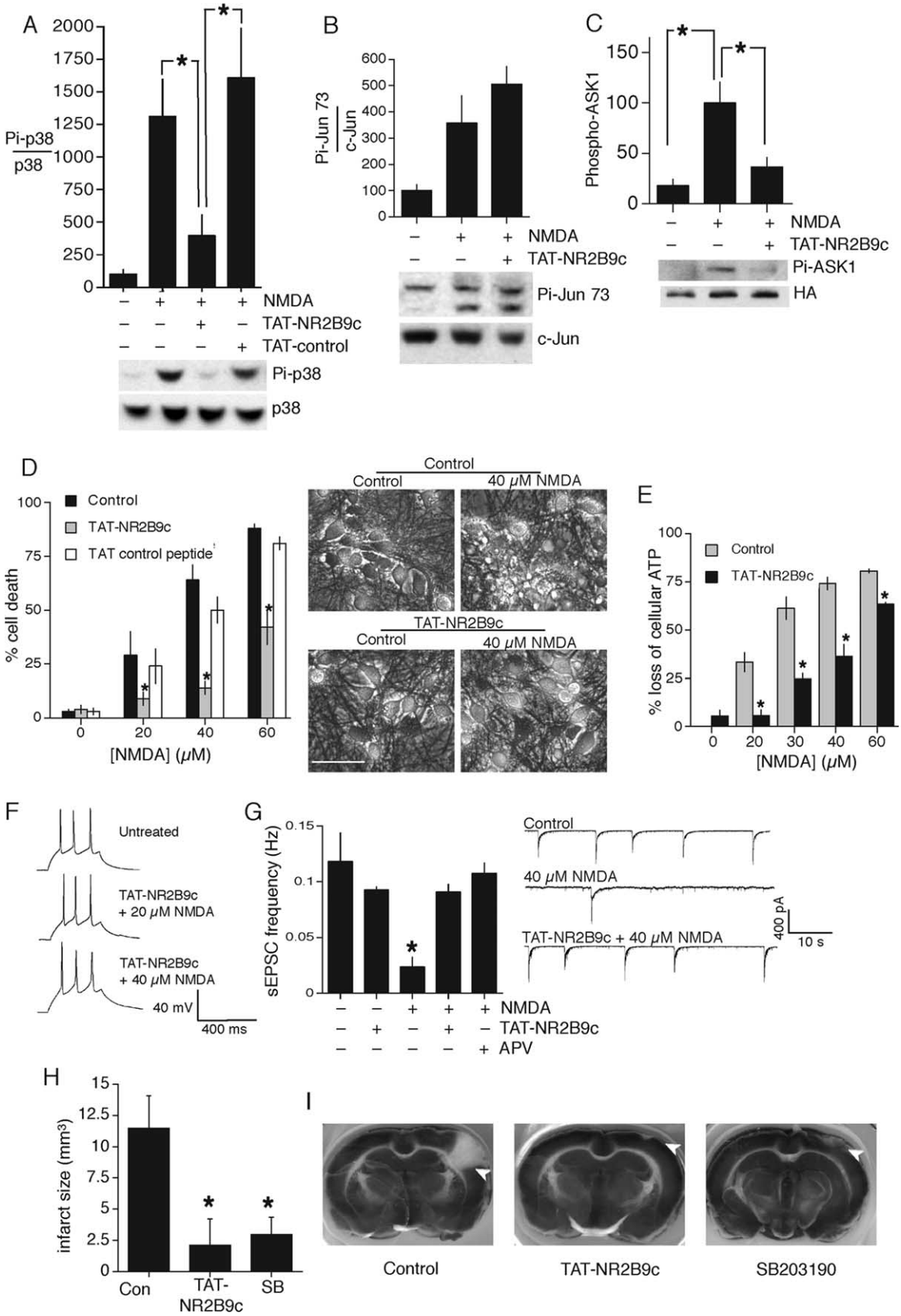

Figure 4. NMDAR signaling to p38 MAPK in neurons is disrupted by a peptide mimetic of the NR2B PDZ ligand. ***A***, TAT-NR2B9c uncouples the NMDAR from p38 activation. Western analysis of p38 activation was performed in cortical neurons stimulated with NMDA (20 μM) for 5 min ($n = 6$). All TAT-peptides were used in this study at 2 μM, and cells were pretreated for 1 h. ***B***, TAT-NR2B9c does not affect NMDAR-dependent JNK signaling. Western analysis of activation of JNK-dependent Jun phosphorylation was performed in cortical neurons stimulated with NMDA (20 μM) for 30 min after pretreatment with TAT-NR2B9c (for 1 h) as indicated ($n = 3$). ***C***, TAT-NR2B9c uncouples the NMDAR from ASK1 activation. Neurons were transfected with pHA-ASK1 and after 24 h stimulated with NMDA (20 μM) and pretreated with vehicle or TAT-NR2B9c ($n = 3$). HA-ASK1 was immunoprecipitated and subject to Western analysis of activation (*Figure legend continues.*)

via p38 inhibition. If this were the case, then the model of focal ischemia amenable to protection by TAT-NR2B9c (Aarts et al., 2002) should cause brain damage that is p38 dependent. We performed the three pial vessel occlusion (3PVO) model of focal ischemia on adult rats, which involves cauterization of three terminal pial branches of the middle cerebral artery. Brain injury after 3PVO is nearly completely protected by treatment with TAT-NR2B9c (Fig. 4*H*,*I*). We then tested the effect of administering the p38 inhibitor SB202190 and found that this too offered very strong protection against brain damage after 3PVO (Fig. 4*H*,*I*; supplemental Fig. S2, available at www.jneurosci.org as supplemental material), suggesting that TAT-NR2B9c and the p38 inhibitor may be acting on a common pathway *in vivo*, as is the case *in vitro*.

TAT-NR2B9c does not block survival or plasticity signaling, unlike conventional NMDAR antagonists

An aim of this study is to determine whether the NMDAR can be uncoupled from pro-death signaling without impairing prosurvival signaling, or synaptic plasticity. We first investigated the effect of TAT-NR2B9c on PI3K–Akt signaling and activation of cAMP response element-binding protein (CREB)-dependent gene expression, key mediators of synaptic NMDAR-dependent neuroprotection (Papadia et al., 2005; Hardingham, 2006). TAT-NR2B9c did not impair activation of CREB-dependent reporter activation triggered by an episode of synaptic NMDAR activity lasting 1 h or 30 min (Fig. 5*A* and data not shown). In fact, TAT-NR2B9c had a small but significant potentiating effect (Fig. 5*A*), the basis for which is not clear. Consistent with an absence of a role for either p38 or JNK in activity-dependent CREB activation, neither SB203580 nor SP600125 impaired activation of the CRE reporter (data not shown). TAT-NR2B9c also did not interfere with activity-dependent induction of a CREB target gene *Adcyap1* (Fukuchi et al., 2005), which encodes the neuroprotective ligand PACAP (pituitary adenylate cyclase-activating polypeptide; data not shown). TAT-NR2B9c had no effect on synaptic NMDAR signaling to Akt activation triggered by an episode of synaptic NMDAR activity lasting 1 h or 30 min (Fig. 5*B* and data not shown). The NMDAR antagonist MK-801 promotes apoptotic-like neurodegeneration in trophically deprived conditions (Papadia et al., 2005). However, TAT-NR2B9c did not promote neuronal death, in contrast to MK-801 (Fig. 5*C*).

We next sought to determine whether TAT-NR2B9c impaired NMDAR-dependent synaptic plasticity. We used a neuronal culture model of plasticity (Arnold et al., 2005) in which a brief period of bicuculline-induced bursting causes an NMDAR-dependent increase in mEPSC frequency in hippocampal neurons (for example traces, see Fig. 5*D*,*E*), attributed to AMPA receptor insertion and unsilencing of synapses (Abegg et al., 2004). We found that, whereas MK-801 blocked the increase in mEPSC frequency, TAT-NR2B9c had no effect (Fig. 5*D*,*E*). SP600125 did not suppress the synaptic NMDAR-dependent enhancement of mEPSC frequency; however, SB203580 did have an inhibitory effect (data not shown). Thus, TAT-NR2B9c has a

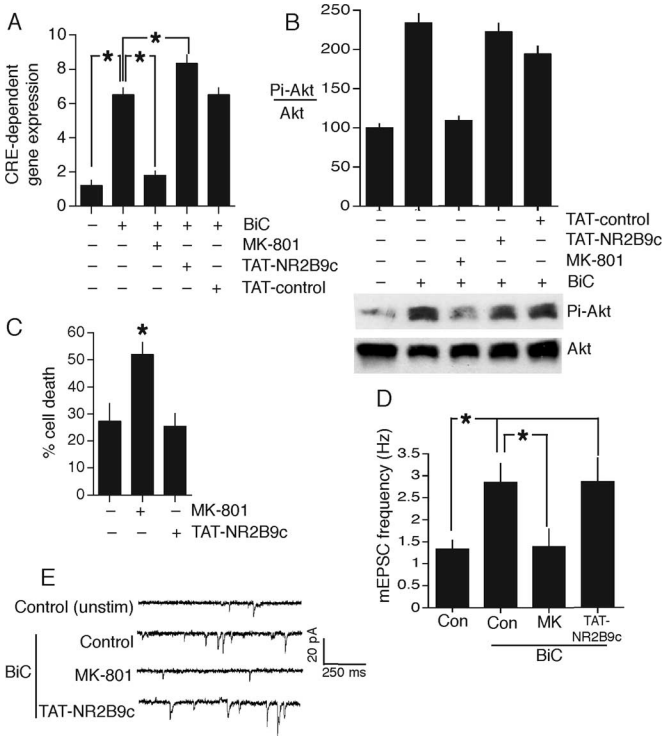

Figure 5. TAT-NR2B9c does not block survival or plasticity signaling, unlike conventional NMDAR antagonists. ***A***, TAT-NR2B9c does not impair synaptic NMDAR-dependent activation of a CRE reporter. Neurons were transfected with a CRE-firefly luciferase vector plus pTK-*Renilla* transfection control. Twenty-four hours after transfection, neurons were pretreated with the peptides (2 μM) or MK-801 (10 μM) for 1 h before bicuculline (BiC) stimulation for 1 h. After 1 h, synaptic activity was terminated by TTX (1 μM) and MK-801 (10 μM), and luciferase expression was measured after a further 6–7 h. CRE-firefly luciferase activity is normalized to *Renilla* control ($n = 3$). ***B***, TAT-NR2B9c does not impair synaptic NMDAR-dependent activation of Akt. Shown is Western analysis of Akt activation by bicuculline treatment, and the effect of the indicated peptides and drugs ($n = 3$). ***C***, TAT-NR2B9c does not promote neuronal apoptosis, unlike MK-801. Neurons were placed in trophically deprived medium and treated with vehicle, MK-801, or TAT-NR2B9c for 72 h before fixation and DAPI staining. In the case of TAT-NR2B9c, fresh peptide was added every 24 h. The number of DAPI-stained apoptotic-like nuclei as a percentage of the total was calculated ($n = 4$). ***D***, TAT-NR2B9c does not block NMDAR-dependent synaptic plasticity. Hippocampal neurons were pretreated for 1 h with peptide or MK-801 as indicated and in the presence of these compounds were treated with medium with or without bicuculline for 15 min and then allowed to settle for 30 min. mEPSCs were then recorded for 5–10 min (minimum 300 events), and the frequency was calculated ($n = 8$–10 for each condition). Con, Control. ***E***, Examples of traces used to generate the data shown in ***D***. unstim, Unstimulated.

←

(*Figure legend continued.*) of ASK1, measured by analyzing ASK1 (Thr-845) phosphorylation. ***D***, TAT-NR2B9c protects neurons against NMDAR-dependent excitotoxic cell death. Neurons treated with TAT-NR2B9c or control peptide for 1 h before excitotoxic insult (NMDA) for 1 h. Left, Neuronal loss assessed after 24 h by DAPI staining and counting pyknotic nuclei ($n = 3$). Right, Phase-contrast pictures illustrating the protective effects of TAT-NR2B9c. Scale bar, 50 μm. Note the phrase-bright cell debris from dead neurons in the control cultures treated with 40 μM NMDA (top right). ***E***, TAT-NR2B9c protects neurons against NMDAR-dependent excitotoxic cell death as assayed by loss of cellular ATP. Neurons were treated as in ***D***, and after 24 h, cellular ATP levels were measured by CellTiter-Glo assay (Promega; $n = 4$). ***F***, Neurons that are protected from NMDA toxicity by TAT-NR2B9c pretreatment fire action potentials as normal. Neurons were treated as indicated using the same protocol as in ***D***. Twenty-four hours after 40 μM NMDA exposure, surviving cells were patched under current clamp. Current was then injected (300 ms pulses at 1 Hz) until depolarized beyond -40 mV. Examples show the firing response that was triggered. ***G***, Neurons that are protected from NMDA toxicity by TAT-NR2B9c pretreatment experience normal levels of synaptic activity. Neurons were treated as indicated using the same protocol as in ***D***. Twenty-four hours after 40 μM NMDA (or vehicle) exposure, surviving cells were recorded under voltage clamp. sEPSC frequency of the neurons was then measured over 3 min of recording time (analysis shown on left, example traces on right).*$p < 0.05$ compared with control neurons ($n = 7$). ***H***, TAT-NR2B9c and the p38 inhibitor SB202190 reduce infarct size in the 3PVO model of stroke. Adult rats were treated with TAT-NR2B9c (7.5 mg/kg) or the p38 inhibitor SB202190 (30 mg/kg) intravenously via a tail vein cannula 15 min before ischemia (3PVO; see Materials and Methods). Animals were killed 24 h after ischemia, and coronal brain slices were taken for analysis of infarct size ($n = 8$ for each group). Con, Control. ***I***, Example brain slices (analysis in ***H***) stained in 2% triphenyltetrazolium chloride; infarcts are highlighted with white arrowheads.

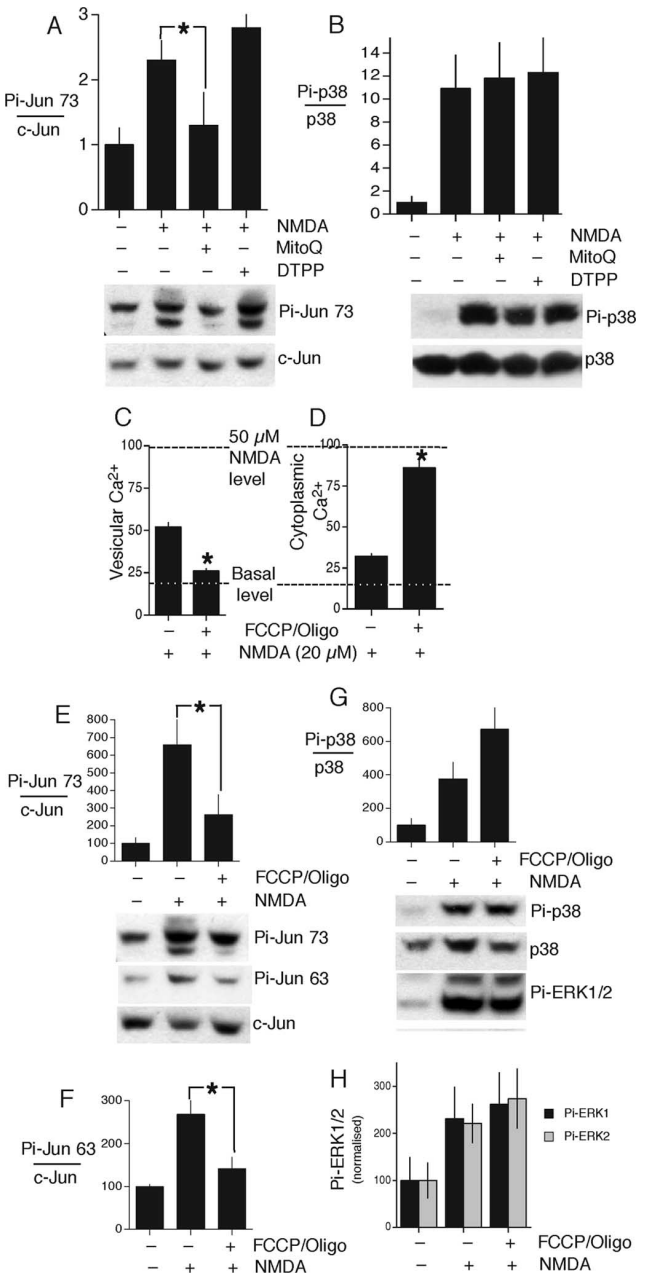

Figure 6. JNK activation involves mitochondria. ***A***, ***B***, MitoQ blocks NMDAR-dependent JNK signaling, but not p38 activation. Shown is Western analysis of NMDAR-mediated JNK-dependent Jun phosphorylation (***A***) and p38 activation (***B***) in neurons pretreated for 1 h with vehicle, MitoQ (5 μM), or DTPP control (5 μM) ($n = 4$). ***C***, Predepolarization of mitochondria blocks NMDA-induced vesicular Ca^{2+} uptake. Neurons were pretreated (for 5 min) where indicated with F/O before stimulation and measurement of vesicular $^{45}Ca^{2+}$ uptake ($n = 3$). ***D***, Predepolarization of mitochondria causes an increase in NMDA-induced cytoplasmic Ca^{2+} load. Neurons were pretreated where indicated with F/O before stimulation and measurement of cytoplasmic $^{45}Ca^{2+}$ uptake ($n = 3$). For reference, the level of cytoplasmic $^{45}Ca^{2+}$ uptake induced by 50 μM NMDA is also shown. ***E–H***, Predepolarization of mitochondria blocks JNK signaling but not p38 or ERK1/2. Shown is an assessment of the effect of F/O pretreatment on NMDA induction of c-Jun phosphorylation on serine-73 (***E***; example blot below) and c-Jun phosphorylation on serine-63 (***F***; example blot above), both normalized to c-Jun levels ($n = 3$), p38 activation (***G***; example blot below; $n = 3$), and ERK1/2 phosphorylation (***H***; example blot above). Phosphorylation levels in ***G*** and ***H*** are normalized to p38.

clear advantage over a global small molecule inhibitor of p38 with regard to unwanted interference with this plasticity model.

We also studied the effect of TAT-NR2B9c on basal activity and found that mEPSC frequency was not altered by TAT-NR2B9c, nor was sEPSC frequency affected (data not shown), indicating that overall excitability of the neuronal network is not altered. Thus, TAT-NR2B9c can impair NMDAR-dependent pro-death signaling, without interfering appreciably with NMDAR-dependent prosurvival signaling or a model of NMDAR-dependent synaptic plasticity.

JNK activation by mitochondrial reactive oxygen species

The JNK dependency of NMDAR-mediated cell death of NR-AtT20 cells revealed that this signaling cassette may not require the NMDAR signaling complex. Consistent with this, TAT-NR2B9c did not interfere with JNK activation (Fig. 4*B*). These observations raise the possibility that the Ca^{2+} effector of JNK activation may be away from the NMDA receptor signaling complex at a different subcellular location. Ca^{2+} uptake into mitochondria, through the potential-driven uniporter, is known to play a role in NMDAR-dependent cell death (Stout et al., 1998) and triggers the production of reactive oxygen species (ROSs) (Nicholls, 2004), regulators of JNK signaling (Torres and Forman, 2003). To investigate the role of mitochondrial ROS production in JNK activation, we treated neurons with the mitochondrially targeted ubiquinone-based antioxidant, MitoQ (Kelso et al., 2001). MitoQ strongly inhibited NMDA-induced JNK signaling (Fig. 6*A*), but not p38 activation (Fig. 6*B*), whereas the targeting moiety (DTPP) had no effect on JNK (Fig. 6*A*). Recently, protein kinase D (PKD; also known as PKCμ) was shown to mediate the activation of JNK signaling by ROS in HEK cells (Eisenberg-Lerner and Kimchi, 2007). To investigate the role of PKCμ/PKD in neurons, we used the established method of applying PKC isoform inhibitors with slightly different specificities (Lemonnier et al., 2004; Zhang et al., 2005; Ivison et al., 2007): 12-(2-cyanoethyl)-6,7,12,13-tetrahydro-13-methyl-5-oxo-5*H*-indolo(2,3-*a*)pyrrolo(3,4-*c*)-carbazole (Gö6976) inhibits multiple isoforms of PKC, including α, β, and μ (PKD) isoforms, whereas 2-[1-(3-dimethylaminopropyl)-5-methoxyindol-3-yl]-3-(1*H*-indol-3-yl)maleimide (Gö6983) blocks PKCα, β, γ, δ, and ζ isoforms, but not PKCμ/PKD. We found that Gö6976, but not Gö6983, inhibited NMDAR-dependent JNK signaling (supplemental Fig. S3, available at www.jneurosci.org as supplemental material). Because PKCμ/PKD is the only known kinase that is inhibited by Gö6976 but not by Gö6983, this implicates PKCμ/PKD in the activation of JNK by NMDAR-dependent mitochondrial ROS production. However, we cannot rule out that any hitherto unknown kinases that are blocked by Gö6976 but not Gö6983 could also be responsible for the effects that we observe.

An implication of the inhibitory effect of MitoQ is that interfering with mitochondrial Ca^{2+} uptake may impair JNK signaling. NMDAR activation induces a dose-dependent increase in vesicular Ca^{2+} load, the majority of which is mitochondrial (Ward et al., 2005). Mitochondrial Ca^{2+} uptake can be prevented by predepolarizing the mitochondria with the uncoupler FCCP, which has been reported to reduce NMDAR-dependent cell death (Stout et al., 1998). We treated neurons with FCCP plus the mitochondrial ATPase inhibitor oligomycin (to prevent depletion of cytoplasmic ATP through ATPase reversal). FCCP/oligomycin (F/O) pretreatment dramatically reduced vesicular Ca^{2+} uptake triggered by 20 μM NMDA (Fig. 6*C*), confirming that most NMDA-induced vesicular Ca^{2+} uptake was into mitochondria [the remainder being into the endoplasmic reticulum (Ward et al., 2005)]. Consistent with a major uptake mechanism being blocked, cytoplasmic Ca^{2+} load triggered by 20 μM NMDA was increased by F/O pretreatment (Fig. 6*D*) to levels similar to those

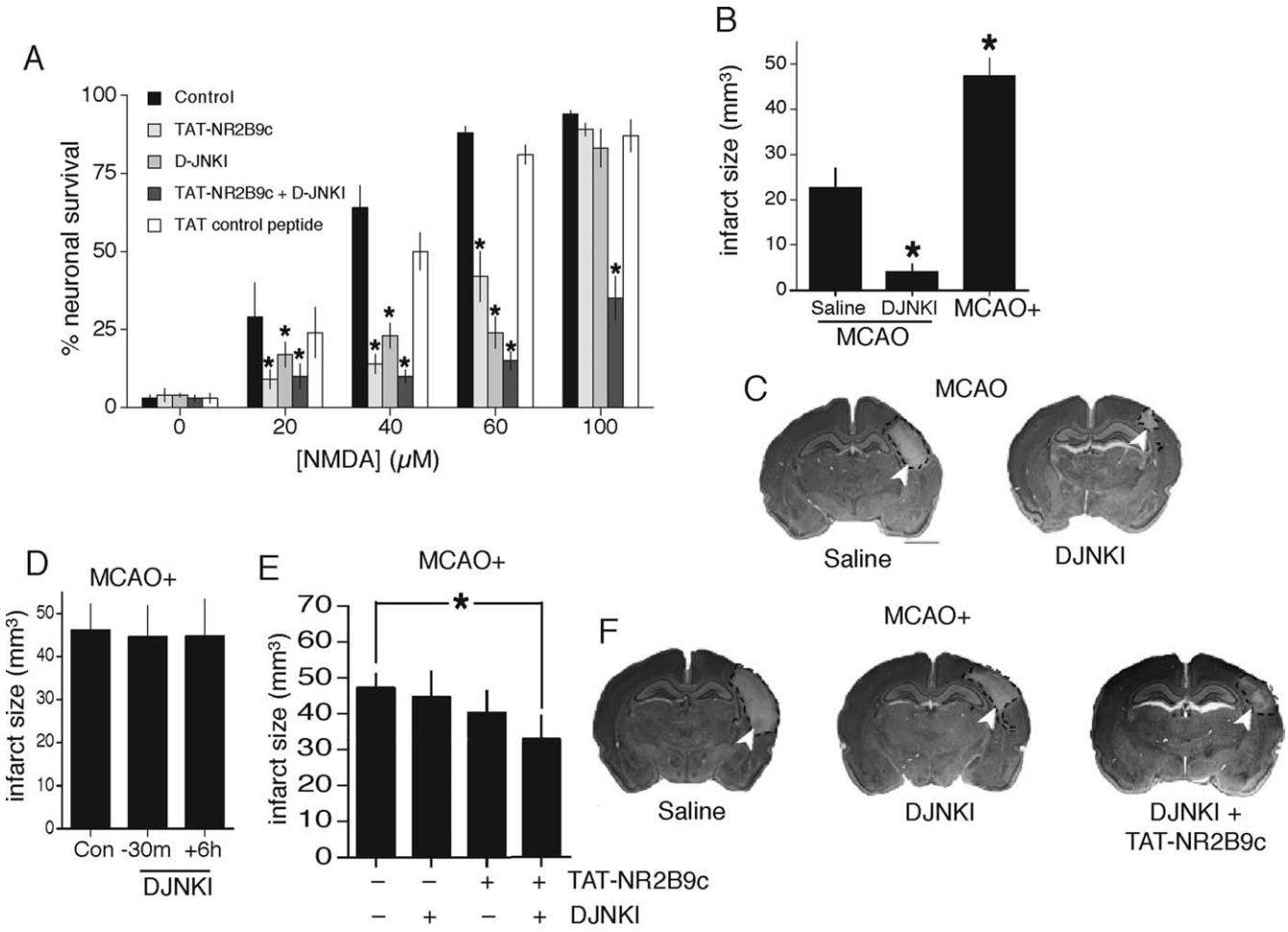

Figure 7. Effective anti-excitotoxic therapy by combining TAT-NR2B9c with a TAT-fused JNK inhibitor *in vitro* and *in vivo*. ***A***, TAT-NR2B9c and D-JNKI1 are additively anti-excitotoxic in neurons *in vitro*. Cortical neurons were pretreated with the indicated peptides for 1 h before excitotoxic insult (NMDA) for 1 h. Neuronal loss was assessed after 24 h ($n = 3$). ***B***, D-JNKI1 provides effective treatment of MCAO alone, and the MCAO+ model results in large infarcts. Saline or D-JNKI1 (0.3 mg/kg, i.p.) was administered 6 h after simple MCAO (*$p < 0.001$, Student's *t* test). For comparison, infarct size caused by severe (MCAO+; see Materials and Methods) model of ischemia is shown. ***C***, Examples of stained slices illustrating the protective effect of D-JNKI1 (see ***B***). Scale bar, 1 mm. ***D***, D-JNKI1 treatment of MCAO+. D-JNKI1 (0.3 mg/kg, i.p., 6 h after MCAO or 30 min before it) does not significantly reduce the infarct volume. Con, Control. ***E***, TAT-NR2B9c and D-JNKI1 are additively protective in the severe MCAO+ stroke model. The graph shows the effects of combined peptide treatment of MCAO+. Neither D-JNKI1 (0.3 mg/kg, i.p.) alone nor TAT-NR2B9c (7.5 mg/kg, i.p.) alone reduced the infarct volume significantly, but combined treatment with both peptides gave significant protection (*$p < 0.05$, Mann–Whitney test). For each treatment, 7–20 animals were used. ***F***, Examples of stained slices analyzed in ***E***. Arrowheads indicate the infarcts.

induced by 50 μM NMDA in the absence of F/O. Indeed, F/O pretreatment inhibited NMDA-induced JNK signaling (Fig. 6*E*,*F*), whereas NMDAR coupling to p38 and ERK1/2 activation was not affected (Fig. 6*G*,*H*).

Effective anti-excitotoxic therapy by combining TAT-NR2B9c with a TAT-fused JNK inhibitor *in vitro* and *in vivo*

Interestingly, we found that TAT-NR2B9c was not neuroprotective at high doses of NMDA (100 μM) (Fig. 7*A*). Given that TAT-NR2B9c interferes with NMDAR pro-death signaling to p38 and not JNK, we hypothesized that both pathways must be blocked to achieve protection after exposure to high doses of NMDA. We tested the neuroprotective effect of TAT-NR2B9c in combination with the cell-permeable peptide JNK inhibitor, D-JNKI1 (Borsello et al., 2003) (Fig. 2*A*). Although either peptide alone was protective against moderate doses of NMDA, neither was effective against 100 μM NMDA. However, when combined they offered significant neuroprotection at 100 μM NMDA (Fig. 7*A*). Thus, both SAPK pathways must be blocked to offer neuroprotection against a severe excitotoxic insult. Although both TAT-NR2B9c and D-JNKI1 protect against models of rodent focal ischemia (Aarts et al., 2002; Borsello et al., 2003), we hypothesized that they may work well in combination *in vivo*. Given the efficacy of these peptides on their own, we sought a severe model of ischemia beyond the protective effects of either peptide individually.

D-JNKI1 alone gives strong protection against focal ischemia caused by MCAO in neonatal rats or adult mice (Borsello et al., 2003), so we created a stronger ischemic insult in P12 rats by combining MCAO with 90 min closure of the ipsilateral common carotid artery (MCAO+) (Renolleau et al., 1998). This produces more complete ischemia, reducing irrigation of the ischemic zone by anastomoses from the anterior and posterior cerebral arteries. MCAO+ resulted in larger infarcts than MCAO (Fig. 7*B*). Furthermore, although D-JNKI1 alone given 6 h after the onset of ischemia reduced the infarct volume in the MCAO model (Fig. 7*B*,*C*), the same dose given either 30 min before or 6 h after the MCAO+ procedure was ineffective (Fig. 7*D*). The effects of TAT-NR2B9c alone or in combination with D-JNKI1 were also tested. Because the therapeutic window for D-JNKI1 is

12 h (Borsello et al., 2003), we administered D-JNKI1 at 6 h after the onset of ischemia. TAT-NR2B9c was given 30 min before ischemia, because the therapeutic window for its use was unknown. TAT-NR2B9c alone did not significantly reduce the volume of the infarct, but its combination with D-JNKI1 gave significant protection (Fig. 7*E*,*F*; supplemental Fig. S4, available at www.jneurosci.org as supplemental material). Therefore, inhibiting NMDAR pro-death signals that are both dependent on the NSC (p38) and independent of it (JNK) has synergistically protective effects in severe excitotoxic scenarios *in vitro* and *in vivo*.

Discussion

We show here that the NMDAR can be uncoupled from pro-death signaling without interfering in models of synaptic NMDAR-dependent neuroprotection and synaptic plasticity. We also demonstrate that NMDAR signaling to JNK and p38 has differing dependencies on neuron-specific signaling proteins and the NR2B PDZ ligand, yet both contribute to excitotoxic death. Targeting both pathways relies on separate approaches and provides effective protection from excitotoxicity *in vitro* and *in vivo*.

Failed clinical trials for stroke with NMDAR antagonists

Despite evidence from animal studies implicating the NMDAR in ischemic brain damage, clinical trials of NMDAR antagonists for stroke have failed because of poor tolerance and efficacy (Ikonomidou and Turski, 2002; Muir, 2006). The important role of NMDARs in the CNS may mean that for any antagonist, the maximal tolerated dose is lower than the therapeutically effective dose, because many unacceptable side effects are on-target effects. Evidence that NMDAR activity can exert a neuroprotective effect has led to suggestions that it may even promote recovery after reperfusion, and prevent delayed neuronal loss in the penumbra (Albers et al., 2001; Ikonomidou and Turski, 2002). As such, antagonists may be protective early in the insult but not later on, which indicates a potential need for more specific anti-excitotoxic strategies in which the effects on prosurvival NMDAR signaling are considered.

NMDAR-activated survival and death signals require spatially distinct pools of Ca^{2+}

Activation of CREB is an important mediator of synaptic NMDAR-dependent neuroprotection (Papadia et al., 2005). Elevation of Ca^{2+} within the nucleus is important for full activation of CREB-dependent gene expression and resultant neuroprotection (Hardingham et al., 1997, 2001a; Papadia et al., 2005), likely because of the nuclear localization of CREB's activator CaMKIV. Nuclear Ca^{2+} is also implicated in regulating memory consolidation (Limbäck-Stokin et al., 2004), although whether this is via CREB activation is not known. Thus, the nucleus is a major site for physiological effects of NMDAR signaling. However, it does not appear to play a role in excitotoxic cell death, because inhibition of nuclear Ca^{2+}/calmodulin signaling does not interfere with NMDAR-dependent excitotoxic cell death (G. E. Hardingham, unpublished work). Another key NMDAR-activated prosurvival signal, the PI3K–Akt pathway (Hetman and Kharebava, 2006), is likely to be activated by cytoplasmic Ca^{2+} elevation, because of the Ca^{2+}/calmodulin dependence of PI3K (Joyal et al., 1997). Our results support this, because submembranous Ca^{2+} is insufficient to trigger this pathway (Fig. 3*D*,*F*). On the other hand, submembranous Ca^{2+} transients are sufficient to activate p38 signaling (Fig. 3*D*,*E*), which is a Ca^{2+} pool not involved in either prosurvival pathway. In contrast, pro-death signaling via JNK may directly or indirectly involve Ca^{2+} uptake into mitochondria and mitochondrial ROS production (Fig. 6). Ca^{2+} uptake into mitochondria has been shown to trigger ROS production (Nicholls, 2004), suggesting that mitochondrial ROS generation, potentially triggered by mitochondrial Ca^{2+} uptake, is a trigger for JNK signaling. Thus in cortical neurons, the NMDAR-activated effectors of survival and death have very different spatial requirements for Ca^{2+}.

Role of the NR2B PDZ ligand in death signaling

The cell-permeable TAT-based NR2B9c fusion peptide protects against excitotoxicity *in vitro* and *in vivo* by uncoupling NR2B from PSD-95 and downstream signaling molecules such as nNOS (Aarts et al., 2002) and p38 MAP kinase (this study). Moreover, a model of ischemia in which TAT-NR2B9c is highly neuroprotective is also responsive to a p38 inhibitor (Fig. 4*H*,*I*), suggesting that TAT-NR2B9c acts *in vivo* by impairing pro-death p38 signaling. Despite its efficacy, TAT-NR2B9c would be of limited benefit over conventional NMDAR antagonists if it impaired physiological prosurvival and plasticity signaling. However, at therapeutic concentrations, TAT-NR2B9c did not interfere with neuronal culture models of these processes, nor did it affect basal network activity. The fact that TAT-NR2B9c did not impair Ca^{2+} influx nor affect our model of NMDAR-dependent synaptic plasticity suggests that interactions with the NR2B PDZ ligand may be dispensable for plasticity, at least in the short term (although effects on other models of plasticity cannot be ruled out).

Although global NMDAR blockade is not thought to be a viable therapeutic option, a specific role for NR2B-NMDARs in promoting cell death has been suggested (Liu et al., 2007) and would enable this particular subtype of NMDAR to be targeted without impairing prosurvival signaling, using the highly selective antagonists available. However, we recently found that NR2B-NMDARs are capable of promoting both survival and death signaling (Martel et al., 2008). Interestingly, NMDARs have been reported to mediate p38 dephosphorylation in hippocampal neurons (Krapivinsky et al., 2004; Waxman and Lynch, 2005) mediated by NR2B-NMDARs (Waxman and Lynch, 2005), which is presumably a protective response that NR2B antagonists would block. Moreover, NR2A-NMDARs were recently shown to be capable of mediating excitotoxicity as well as protective signaling (von Engelhardt et al., 2007). Together, these studies indicate that NR2B-NMDARs and NR2A-NMDARs are both capable of mediating survival and death signaling. Thus, the specific ability of NR2B-NMDARs and NR2A-NMDARs to promote death and survival, respectively (Liu et al., 2007), may not apply in all neuronal types at all developmental stages.

The inability of TAT-NR2B9c to uncouple the NMDAR from JNK signaling (Fig. 4*B*) or impair JNK-mediated, NMDAR-dependent death of NR-AtT20 cells (data not shown) indicates that the JNK pathway does not rely heavily on the NR2B PDZ domain. This is consistent with mitochondrial ROS production being the trigger for this pro-death signal, rather than membrane-proximal events. Our data implicate PKD as a potential NMDAR-induced activator of JNK signaling by NMDAR activation (supplemental Fig. S3, available at www.jneurosci.org as supplemental material). ROS can induce JNK signaling in HEK293 cells by activating death-associated protein kinase (DAPK), which in turn activates PKD (Eisenberg-Lerner and Kimchi, 2007). The role of DAPK in JNK activation in our model awaits investigation, but, interestingly, DAPK has been found to contribute to cerebral ischemic injury (Shamloo et al., 2005).

The neuroprotective effects of uncoupling NR2B from PSD-95 provide a convincing explanation for the observation

that Ca^{2+} influx specifically through NMDARs promotes cell death: i.e., that Ca^{2+}-dependent cell death is "source specific" (Tymianski et al., 1993). However, this model is not universally accepted: the idea that simply a high Ca^{2+} load is the main reason for NMDAR-dependent cell death is supported by the fact that cell death can be reconstituted in non-neuronal cells by expressing NMDARs in the absence of their associated signaling complexes (Cik et al., 1993). Our data suggest that both models are partially correct: efficient p38 signaling requires the NMDAR signaling complex and could be viewed as source specific, whereas JNK signaling does not. We did not examine calpain activation in this study: although NMDAR activity is a typical physiological activator of calpains in neurons, it is unclear whether this is because of the high Ca^{2+} load triggered or because of specific coupling via structural molecules. Interestingly, a precedent for the latter exists in the case of focal adhesion kinase, which recruits both calpain and extracellular signal-regulated kinase (ERK), resulting in ERK-mediated phosphorylation and activation of calpain (Wells et al., 2005).

Ca^{2+} influx dependent on intense synaptic NMDAR activation is well tolerated by hippocampal neurons, whereas activation of extrasynaptic NMDARs, either on their own or in the presence of synaptic NMDAR activation, causes a loss of mitochondrial membrane potential and cell death (Hardingham et al., 2002). These findings have been recapitulated by others in cortical neurons (Leveille et al., 2005), raising the possibility that this is a general CNS phenomenon. At first glance, these observations are at apparent odds with the protective effects of TAT-NR2B9c, if we assume that TAT-NR2B9c exerts its effect by uncoupling synaptic NMDARs from PSD-95 and nNOS activation. However, TAT-NR2B9c could conceivably be exerting its effects on extrasynaptic as well as synaptic NMDARs. Although immunohistochemical studies show PSD-95 to be mostly in synaptic puncta, this does not rule out a more diffuse distribution of PSD-95 at extrasynaptic sites, interacting with extrasynaptic NMDARs. Moreover, extrasynaptic clusters of PSD-95 have been observed in hippocampal neurons at a frequency of almost half that of synaptic clusters (Carpenter-Hyland and Chandler, 2006). Another possibility is that extrasynaptic NR2 PDZ ligands form interactions with a death effector other than PSD-95, which are also disrupted by TAT-NR2B9c.

Even if TAT-NR2B9c is acting specifically on synaptic NMDARs, it could be that synaptic NMDAR signaling to p38 contributes to cell death in the context of a neuron experiencing chronic extrasynaptic NMDAR activity. There is a good deal of evidence implicating p38 as a mediator of NMDAR-dependent excitotoxicity (Kawasaki et al., 1997; Cao et al., 2004; Rivera-Cervantes et al., 2004; Molz et al., 2008). However, nontoxic episodes of NMDAR activity (e.g., induced by bicuculline or low doses of NMDA) can also activate p38, indicating that p38 only contributes to toxicity in certain contexts. Thus, it is possible that synaptic NMDAR signaling to p38 is tolerated during an episode of synaptic activity; however, it may be harmful when induced in a cell under stress from chronically elevated levels of extracellular glutamate (e.g., after an ischemic episode).

Another intriguing question surrounding the action of TAT-NR2B9c is whether it is acting via pathways other than simply inhibiting p38 activation. This seems likely, because the protective effect of TAT-NR2B9c is at least as good as that of p38 inhibitors, despite not completely inhibiting p38 activation by NMDA. Other pro-death pathways may be inhibited, for example, other toxic actions of NO production. Alternatively, a lack of protein interactions at the NR2 PDZ ligand may facilitate the binding of other signaling molecules that promote a prosurvival effect.

Future therapy combinations in stroke trials?

Therapies that target downstream death pathways in combination may be effective in blocking NMDAR pro-death signaling, such as a combination of TAT-NR2B9c and D-JNKI, both of which are effective if administered after the commencement of ischemia (Aarts et al., 2002; Borsello et al., 2003). Although in our model, the SAPKs p38 and JNK are the main mediators of excitotoxicity, other mediators of ischemic cell death include calpain-dependent cleavage of the Na^+/Ca^{2+} exchanger (Bano et al., 2005) and activation of TRPM7 channels (Aarts et al., 2003). The precise pathway(s) that mediate ischemic brain damage may depend on the neuronal subtype, the severity and duration of the episode, and the position of the neuron within the ischemic zone (core or penumbra). Therefore, it may be that additional molecules that target calpain or TRPM7 activation may be yet more effective as part of a mixture of antideath signaling drugs. Their use, where appropriate, in conjunction with the thrombolytic drug tissue plasminogen activator, may aid in rapid drug delivery to the site of insult.

References

Aarts M, Liu Y, Liu L, Besshoh S, Arundine M, Gurd JW, Wang YT, Salter MW, Tymianski M (2002) Treatment of ischemic brain damage by perturbing NMDA receptor-PSD-95 protein interactions. Science 298:846–850.

Aarts M, Iihara K, Wei WL, Xiong ZG, Arundine M, Cerwinski W, MacDonald JF, Tymianski M (2003) A key role for TRPM7 channels in anoxic neuronal death. Cell 115:863–877.

Abegg MH, Savic N, Ehrengruber MU, McKinney RA, Gähwiler BH (2004) Epileptiform activity in rat hippocampus strengthens excitatory synapses. J Physiol 554:439–448.

Adams SM, de Rivero Vaccari JC, Corriveau RA (2004) Pronounced cell death in the absence of NMDA receptors in the developing somatosensory thalamus. J Neurosci 24:9441–9450.

Albers GW, Goldstein LB, Hall D, Lesko LM (2001) Aptiganel hydrochloride in acute ischemic stroke: a randomized controlled trial. JAMA 286:2673–2682.

Anegawa NJ, Guttmann RP, Grant ER, Anand R, Lindstrom J, Lynch DR (2000) *N*-methyl-D-aspartate receptor mediated toxicity in nonneuronal cell lines: characterization using fluorescent measures of cell viability and reactive oxygen species production. Brain Res Mol Brain Res 77:163–175.

Arnold FJ, Hofmann F, Bengtson CP, Wittmann M, Vanhoutte P, Bading H (2005) Microelectrode array recordings of cultured hippocampal networks reveal a simple model for transcription and protein synthesis-dependent plasticity. J Physiol 564:3–19.

Arundine M, Tymianski M (2004) Molecular mechanisms of glutamate-dependent neurodegeneration in ischemia and traumatic brain injury. Cell Mol Life Sci 61:657–668.

Bading H, Greenberg ME (1991) Stimulation of protein tyrosine phosphorylation by NMDA receptor activation. Science 253:912–914.

Bading H, Ginty DD, Greenberg ME (1993) Regulation of gene expression in hippocampal neurons by distinct calcium signaling pathways. Science 260:181–186.

Bano D, Young KW, Guerin CJ, Lefeuvre R, Rothwell NJ, Naldini L, Rizzuto R, Carafoli E, Nicotera P (2005) Cleavage of the plasma membrane Na+/Ca2+ exchanger in excitotoxicity. Cell 120:275–285.

Baxter AW, Wyllie DJ (2006) Phosphatidylinositol 3 kinase activation and AMPA receptor subunit trafficking underlie the potentiation of miniature EPSC amplitudes triggered by the activation of L-type calcium channels. J Neurosci 26:5456–5469.

Boeckman FA, Aizenman E (1996) Pharmacological properties of acquired excitotoxicity in Chinese hamster ovary cells transfected with *N*-methyl-D-aspartate receptor subunits. J Pharmacol Exp Ther 279:515–523.

Borsello T, Clarke PG, Hirt L, Vercelli A, Repici M, Schorderet DF, Bogousslavsky J, Bonny C (2003) A peptide inhibitor of c-Jun N-terminal ki-

nase protects against excitotoxicity and cerebral ischemia. Nat Med 9:1180–1186.

Camacho A, Massieu L (2006) Role of glutamate transporters in the clearance and release of glutamate during ischemia and its relation to neuronal death. Arch Med Res 37:11–18.

Cao J, Semenova MM, Solovyan VT, Han J, Coffey ET, Courtney MJ (2004) Distinct requirements for p38alpha and c-Jun N-terminal kinase stress-activated protein kinases in different forms of apoptotic neuronal death. J Biol Chem 279:35903–35913.

Cao J, Viholainen JI, Dart C, Warwick HK, Leyland ML, Courtney MJ (2005) The PSD95-nNOS interface: a target for inhibition of excitotoxic p38 stress-activated protein kinase activation and cell death. J Cell Biol 168:117–126.

Carpenter-Hyland EP, Chandler LJ (2006) Homeostatic plasticity during alcohol exposure promotes enlargement of dendritic spines. Eur J Neurosci 24:3496–3506.

Chohan MO, Iqbal K (2006) From tau to toxicity: emerging roles of NMDA receptor in Alzheimer's disease. J Alzheimers Dis 10:81–87.

Cik M, Chazot PL, Stephenson FA (1993) Optimal expression of cloned NMDAR1/NMDAR2A heteromeric glutamate receptors: a biochemical characterization. Biochem J 296:877–883.

Coffey ET, Smiciene G, Hongisto V, Cao J, Brecht S, Herdegen T, Courtney MJ (2002) c-Jun N-terminal protein kinase (JNK) 2/3 is specifically activated by stress, mediating c-Jun activation, in the presence of constitutive JNK1 activity in cerebellar neurons. J Neurosci 22:4335–4345.

Cui H, Hayashi A, Sun HS, Belmares MP, Cobey C, Phan T, Schweizer J, Salter MW, Wang YT, Tasker RA, Garman D, Rabinowitz J, Lu PS, Tymianski M (2007) PDZ protein interactions underlying NMDA receptor-mediated excitotoxicity and neuroprotection by PSD-95 inhibitors. J Neurosci 27:9901–9915.

Eisenberg-Lerner A, Kimchi A (2007) DAP kinase regulates JNK signaling by binding and activating protein kinase D under oxidative stress. Cell Death Differ 14:1908–1915.

Fujikawa DG, Shinmei SS, Cai B (2000) Kainic acid-induced seizures produce necrotic, not apoptotic, neurons with internucleosomal DNA cleavage: implications for programmed cell death mechanisms. Neuroscience 98:41–53.

Fukuchi M, Tabuchi A, Tsuda M (2005) Transcriptional regulation of neuronal genes and its effect on neural functions: cumulative mRNA expression of PACAP and BDNF genes controlled by calcium and cAMP signals in neurons. J Pharmacol Sci 98:212–218.

Ghatan S, Larner S, Kinoshita Y, Hetman M, Patel L, Xia Z, Youle RJ, Morrison RS (2000) p38 MAP kinase mediates bax translocation in nitric oxide-induced apoptosis in neurons. J Cell Biol 150:335–347.

Gould E, Cameron HA, McEwen BS (1994) Blockade of NMDA receptors increases cell death and birth in the developing rat dentate gyrus. J Comp Neurol 340:551–565.

Hardingham GE (2006) Pro-survival signalling from the NMDA receptor. Biochem Soc Trans 34:936–938.

Hardingham GE, Bading H (2003) The yin and yang of NMDA receptor signalling. Trends Neurosci 26:81–89.

Hardingham GE, Chawla S, Johnson CM, Bading H (1997) Distinct functions of nuclear and cytoplasmic calcium in the control of gene expression. Nature 385:260–265.

Hardingham GE, Arnold FJ, Bading H (2001a) Nuclear calcium signaling controls CREB-mediated gene expression triggered by synaptic activity. Nat Neurosci 4:261–267.

Hardingham GE, Arnold FJ, Bading H (2001b) A calcium microdomain near NMDA receptors: on switch for ERK-dependent synapse-to-nucleus communication. Nat Neurosci 4:565–566.

Hardingham GE, Fukunaga Y, Bading H (2002) Extrasynaptic NMDARs oppose synaptic NMDARs by triggering CREB shut-off and cell death pathways. Nat Neurosci 5:405–414.

Hetman M, Kharebava G (2006) Survival signaling pathways activated by NMDA receptors. Curr Top Med Chem 6:787–799.

Ikonomidou C, Turski L (2002) Why did NMDA receptor antagonists fail clinical trials for stroke and traumatic brain injury? Lancet Neurol 1:383–386.

Ikonomidou C, Bosch F, Miksa M, Bittigau P, Vöckler J, Dikranian K, Tenkova TI, Stefovska V, Turski L, Olney JW (1999) Blockade of NMDA receptors and apoptotic neurodegeneration in the developing brain. Science 283:70–74.

Ikonomidou C, Stefovska V, Turski L (2000) Neuronal death enhanced by *N*-methyl-D-aspartate antagonists. Proc Natl Acad Sci U S A 97:12885–12890.

Ivison SM, Graham NR, Bernales CQ, Kifayet A, Ng N, Shobab LA, Steiner TS (2007) Protein kinase D interaction with TLR5 is required for inflammatory signaling in response to bacterial flagellin. J Immunol 178:5735–5743.

Joyal JL, Burks DJ, Pons S, Matter WF, Vlahos CJ, White MF, Sacks DB (1997) Calmodulin activates phosphatidylinositol 3-kinase. J Biol Chem 272:28183–28186.

Kawasaki H, Morooka T, Shimohama S, Kimura J, Hirano T, Gotoh Y, Nishida E (1997) Activation and involvement of p38 mitogen-activated protein kinase in glutamate-induced apoptosis in rat cerebellar granule cells. J Biol Chem 272:18518–18521.

Kelso GF, Porteous CM, Coulter CV, Hughes G, Porteous WK, Ledgerwood EC, Smith RA, Murphy MP (2001) Selective targeting of a redox-active ubiquinone to mitochondria within cells: antioxidant and antiapoptotic properties. J Biol Chem 276:4588–4596.

Krapivinsky G, Medina I, Krapivinsky L, Gapon S, Clapham DE (2004) SynGAP-MUPP1-CaMKII synaptic complexes regulate p38 MAP kinase activity and NMDA receptor-dependent synaptic AMPA receptor potentiation. Neuron 43:563–574.

Lemonnier J, Ghayor C, Guicheux J, Caverzasio J (2004) Protein kinase C-independent activation of protein kinase D is involved in BMP-2-induced activation of stress mitogen-activated protein kinases JNK and p38 and osteoblastic cell differentiation. J Biol Chem 279:259–264.

Leveille F, Nicole O, Buisson A (2005) Cellular location of NMDA receptors influences their implication in excitotoxic injury. Soc Neurosci Abstr 31:946.2.

Limbäck-Stokin K, Korzus E, Nagaoka-Yasuda R, Mayford M (2004) Nuclear calcium/calmodulin regulates memory consolidation. J Neurosci 24:10858–10867.

Liu Y, Wong TP, Aarts M, Rooyakkers A, Liu L, Lai TW, Wu DC, Lu J, Tymianski M, Craig AM, Wang YT (2007) NMDA receptor subunits have differential roles in mediating excitotoxic neuronal death both *in vitro* and *in vivo*. J Neurosci 27:2846–2857.

Martel M, Wyllie DJ, Hardingham GE (2008) In developing hippocampal neurons, NR2B-containing *N*-methyl-D-aspartate receptors (NMDARs) can mediate signaling to neuronal survival and synaptic potentiation, as well as neuronal death. Neuroscience, doi:10.1016/j.neuroscience.2008.01.080.

McKenzie GJ, Stevenson P, Ward G, Papadia S, Bading H, Chawla S, Privalsky M, Hardingham GE (2005) Nuclear Ca2+ and CaM kinase IV specify hormonal- and Notch-responsiveness. J Neurochem 93:171–185.

Molz S, Decker H, Dal-Cim T, Cremonez C, Cordova FM, Leal RB, Tasca CI (2008) Glutamate-induced toxicity in hippocampal slices involves apoptotic features and p38(MAPK) signaling. Neurochem Res 33:27–36.

Muir KW (2006) Glutamate-based therapeutic approaches: clinical trials with NMDA antagonists. Curr Opin Pharmacol 6:53–60.

Nicholls DG (2004) Mitochondrial dysfunction and glutamate excitotoxicity studied in primary neuronal cultures. Curr Mol Med 4:149–177.

Olney JW (1969) Brain lesions, obesity, and other disturbances in mice treated with monosodium glutamate. Science 164:719–721.

Papadia S, Hardingham GE (2007) The dichotomy of NMDA receptor signaling. Neuroscientist 13:572–579.

Papadia S, Stevenson P, Hardingham NR, Bading H, Hardingham GE (2005) Nuclear Ca^{2+} and the cAMP response element-binding protein family mediate a late phase of activity-dependent neuroprotection. J Neurosci 25:4279–4287.

Papadia S, Soriano FX, Léveillé F, Martel MA, Dakin KA, Hansen HH, Kaindl A, Sifringer M, Fowler J, Stefovska V, McKenzie G, Craigon M, Corriveau R, Ghazal P, Horsburgh K, Yankner BA, Wyllie DJ, Ikonomidou C, Hardingham GE (2008) Synaptic NMDA receptor activity boosts intrinsic antioxidant defenses. Nat Neurosci 11:476–487.

Renolleau S, Aggoun-Zouaoui D, Ben-Ari Y, Charriaut-Marlangue C (1998) A model of transient unilateral focal ischemia with reperfusion in the P7 neonatal rat: morphological changes indicative of apoptosis. Stroke 29:1454–1460; discussion 1461.

Rivera-Cervantes MC, Torres JS, Feria-Velasco A, Armendariz-Borunda J, Beas-Zárate C (2004) NMDA and AMPA receptor expression and cortical neuronal death are associated with p38 in glutamate-induced excitotoxicity in vivo. J Neurosci Res 76:678–687.

Rutter AR, Stephenson FA (2000) Coexpression of postsynaptic density-95 protein with NMDA receptors results in enhanced receptor expression together with a decreased sensitivity to L-glutamate. J Neurochem 75:2501–2510.

Shamloo M, Soriano L, Wieloch T, Nikolich K, Urfer R, Oksenberg D (2005) Death-associated protein kinase is activated by dephosphorylation in response to cerebral ischemia. J Biol Chem 280:42290–42299.

Stout AK, Raphael HM, Kanterewicz BI, Klann E, Reynolds IJ (1998) Glutamate-induced neuron death requires mitochondrial calcium uptake. Nat Neurosci 1:366–373.

Takeda K, Matsuzawa A, Nishitoh H, Tobiume K, Kishida S, Ninomiya-Tsuji J, Matsumoto K, Ichijo H (2004) Involvement of ASK1 in Ca2+-induced p38 MAP kinase activation. EMBO Rep 5:161–166.

Tashiro A, Sandler VM, Toni N, Zhao C, Gage FH (2006) NMDA-receptor-mediated, cell-specific integration of new neurons in adult dentate gyrus. Nature 442:929–933.

Torres M, Forman HJ (2003) Redox signaling and the MAP kinase pathways. Biofactors 17:287–296.

Tovar KR, Westbrook GL (1999) The incorporation of NMDA receptors with a distinct subunit composition at nascent hippocampal synapses *in vitro*. J Neurosci 19:4180–4188.

Tymianski M, Charlton MP, Carlen PL, Tator CH (1993) Source specificity of early calcium neurotoxicity in cultures embryonic spinal neurons. J Neurosci 13:2085–2104.

von Engelhardt J, Coserea I, Pawlak V, Fuchs EC, Köhr G, Seeburg PH, Monyer H (2007) Excitotoxicity in vitro by NR2A- and NR2B-containing NMDA receptors. Neuropharmacology 53:10–17.

Ward MW, Kushnareva Y, Greenwood S, Connolly CN (2005) Cellular and subcellular calcium accumulation during glutamate-induced injury in cerebellar granule neurons. J Neurochem 92:1081–1090.

Waxman EA, Lynch DR (2005) *N*-methyl-D-aspartate receptor subtype mediated bidirectional control of p38 mitogen-activated protein kinase. J Biol Chem 280:29322–29333.

Wells A, Huttenlocher A, Lauffenburger DA (2005) Calpain proteases in cell adhesion and motility. Int Rev Cytol 245:1–16.

Zhang SJ, Steijaert MN, Lau D, Schütz G, Delucinge-Vivier C, Descombes P, Bading H (2007) Decoding NMDA receptor signaling: identification of genomic programs specifying neuronal survival and death. Neuron 53:549–562.

Zhang W, Zheng S, Storz P, Min W (2005) Protein kinase D specifically mediates apoptosis signal-regulating kinase 1-JNK signaling induced by H2O2 but not tumor necrosis factor. J Biol Chem 280:19036–19044.